JAEA-Technology
2006-019

JP0650355

JAEA-Technology

Small Specimen Test Technology of Fracture Toughness in Structural Material F82H Steel for Fusion Nuclear Reactors

Eiichi WAKAI, Hideo OHTSUKA, Shingo MATSUKAWA
Masami ANDO and Shiro JITSUKAWA

Division of Fuels and Materials Engineering
Nuclear Science and Engineering Directorsate

March 2006

Japan Atomic Energy Agency

日本原子力研究開発機構

JAEA-Technology 2006 - 019

Small Specimen Test Technology of Fracture Toughness in Structural Material F82H Steel for Fusion Nuclear Reactors

Eiichi WAKAI, Hideo OHTSUKA, Shingo MATSUKAWA*, Masami ANDO+ and Shiro JITSUKAWA

Division of Fuels and Materials Engineering
Nuclear Science and Engineering Directorate
Japan Atomic Energy Agency
Tokai-mura, Naka-gun, Ibaraki-ken

(Received January 27, 2006)

Small specimen test technology (SSTT) has been developed to investigate mechanical properties of nuclear materials. SSTT has been driven by limited availability of effective irradiation volumes in test reactors and accelerator-based neutron and charged particle sources, and it is very useful for the reduction of waste materials produced in nuclear engineering. In this study new bend test machines have been developed to obtain fracture behaviors of F82H steel for very small bend specimens of pre-cracked t/2-1/3CVN (Charpy V-notch) with 20 mm-length and DFMB (deformation and fracture mini bend specimen) with 9 mm-length and disk compact tension of 0.18DCT type, and fracture behaviors were examined to evaluate DBTT (ductile-brittle transition temperature) at temperatures from -180 to 25°C. The effect of specimen size on DBTT of F82H steel was also examined by using Charpy type specimens such as 1/2t-CVN, 1/3CVN and t/2-1/3CVN. In this paper, it also provides the information of the specimens irradiated at 250°C and 350°C to about 2 dpa in the capsule of 04M-67A and 04M-68A of JMTR experiments.

Keywords: Small Specimen Test Technology, SSTT, Small Bend Specimen, Ductile-brittle Transition Temperature, DBTT, DFMB, JMTR, Fracture Toughness, Effect of Specimen Size, Charpy, Irradiation

---

+ Division of Fusion Energy Technology, Fusion Research and Development Directorate.
* JFE-Techno-Research Corporation

JAEA-Technology 2006 - 019

核融合炉構造材 F82H 鋼の小型破壊靭性試験片等を用いた強度評価技術

日本原子力研究開発機構 原子力基礎工学研究部門 燃料・材料工学ユニット
若井 栄一、大塚 英男、松川 真吾*、安堂 正己+、實川 資朗

(2006 年 1 月 27 日受理)

放射性廃棄物量の低減と国際核融合照射施設（IFMIF）のコンポーネント材料評価などのために、微小破壊靭性試験片を用いた強度特性評価及び微小試験片用小型破壊靭性試験装置の開発を実施した。本報告書では、核融合炉用構造材料として開発した F82H 鋼(Fe-8Cr-2W-0.1C 系マルテンサイト鋼)を用いて、微小破壊靭性試験片作製法やこの微小試験片の靭性評価に及ぼす試験片サイズの効果、並びに、動的及び静的な試験方法による延性脆性遷移温度に関する研究成果とそのために開発した試験装置の性能などを纏めたものである。また、これら微小破壊靭性試験片を用いて、2005 年に約 2dpa まで JMTR 炉で中性子照射した試料の情報を纏めた。

原子力科学研究所（駐在）：〒319-1195 茨城県那珂郡東海村白方白根 2-4
+： 核融合研究開発部門核融合エネルギー工学研究開発ユニット
*： JFE テクノリサーチ株式会社

Contents

目次

1. Mechanical Properties of Small Size Specimens of F82H Steel

1.1 Research Background and The Purpose of This Study

Small specimen test technology (SSTT) has been developed to investigate mechanical properties of nuclear materials. SSTT was driven by limited availability of effective irradiation volumes in test reactors and accelerator-based neutron and charged particle sources [1-5]. The most recent efforts in fracture SSTT have been pursued within the framework of the master curves-shifts method proposed by Odette and co-workers for bcc alloys such as ferritic/martensitic steels currently being considered as the first candidate for fusion reactor structures [6-7]. The master curves-shifts represent a significant extension and modification of recent developments in measuring cleavage initiation toughness for heavy section component integrity assessments. The success in utilizing small specimens to obtain meaningful and useful fracture toughness information is leading to an even more aggressive approach to reducing fracture specimen sizes. A variety of tests have been devised to extract mechanical property data from existing small volume specimens, such as tensile, low and high cycle fatigue, fracture toughness, fatigue crack growth, pressurized tubes, notched and pre-cracked impact specimens and 3 mm diameter disks. A subsets of these specimens and techniques have been tentatively selected as candidates for materials response verification in the IFMIF (international fusion materials irradiation facility), which is a D-Li based high energy neutron source currently undergoing conceptual design [8].

In this study, we have examined the fracture toughness of F82H steel using three type specimens of 0.18DCT (Disk compact tension), pre-cracked t/2-1/3CVN (Charpy V-notch), which is denoted as t/2-1/3PCCVN, with 20 mm-length and DFMB (deformation and fracture mini bend specimen) with 9 mm-length. The 0.18DCT and 1/3CVN specimen is recently used for a standard fracture specimen of the neutron irradiation study in RAF (Reduced-activation ferritic) steels. But the volumes of 0.18DCT and 1/3CVN specimens are not so small in the space of irradiation facility such as IFMIF. It is very important to reduce the specimen volume for the performance of irradiation dose. The blanket structure of fusion reactors will be composed of RAF steel plates and pipes with different thickness, and we should check the dependence of specimen size on the properties of fracture toughness. The t/2-CVN specimen reduced the width of 1/3CVN specimen by half, and the DFMB specimen reduced the width and length of 1/3CVN by about half.

A new bend test machine has manufactured to obtain fracture behavior for very small bend specimens of t/2-1/3PCCVN and DFMB. The fracture behaviors of F82H steel with different type of shapes have been examined. The types of specimens used in this study are 0.18DCT, 1/3CVN, t/2-1/3CVN, t/2-1/3PCCVN, DFMB and SP (small punch) specimens. The purpose of this study is (1) to manufacture fracture toughness testing machines for the small specimens of DFMB and t/2-1/3PCCVN and to check the fracture behaviors of F82H-std steel at RT and (2) to examine the effect of specimen size on DBTT (ductile-brittle transition temperature) of F82H-std steel.

1.2 Fabrication of DFMB, t/2-1/3PCCVN and 0.18DCT Specimens

The fatigue pre-cracks of 0.18DCT, t/2-1/3PCCVN and DFMB specimens were induced by using a fatigue testing machine of Shimazu Lab-5u. The 0.18DCT specimens (12.5 mm diameter and 4.63 mm thickness) were machined in the T-L orientation so that crack propagation occurred parallel to the rolling direction. Fatigue pre-cracking was performed at room temperature in a condition of crack length to specimen width ratio (a/W) of approximately 0.46. This was followed by side-grooving on each side to the depth of ~10% of specimen thickness. The length of fatigue pre-crack extension of 0.18DCT specimen was about 1.3 – 1.4 mm. The applied load at the first step was changed between 108 and 1079 N at 40 Hz. and it was changed between 88 and 883 N at the next step. In the t/2-1/3PCCVN and DFMB specimens, the precrack was induced in the plate shape with V-notch and U-notch, respectively, and the size of the plates was 20 mm x 20 mm square and 3.3 mm in thickness. The depth and angle of V-notch in the t/2-1/3PCCVN were 0.51 mm and 30°, respectively. In the DFMB specimen, U-notch was adopt to reduce the notch region by using a 0.15 mm wire cutter, and the depth and width of U-notch was about 0.5 mm and about 0.2 mm, respectively. The load of the plate for the preparation of t/2-1/3PCCVN and DFMB specimens was changed from 294 to 2942 N at 40 Hz. After the pre-crack procedure, the plate was sliced to about 1.7 mm in thickness by wire cutting. The lengths of the pre-crack of t/2-1/3PCCVN and DFMB specimens were about 0.9 mm and about 0.3 mm, respectively. The ratio of crack length to specimen thickness, a/W, for the DFMB and t/2-1/3PCCVN specimens was controlled to the values from 0.40 to 0.45. The chemical compositions of the specimens in this study are given in Table 1.

1.3 Fracture Toughness Testing

1.3.1 Fracture Toughness Testing of DFMB and t/2-1/3PCCVN

Fig. 1.1 shows a new bend test machine, which is manufactured to obtain fracture behavior for very small bend specimens of t/2-1/3PCCVN with 20 mm-length (W: 3.3 mm, H: 1.65 mm) and DFMB with 9 mm-length (W: 1.65 mm, H: 1.65 mm). The displacement rates of cross head in this machine can be changed from 0.01 mm/min to 100 mm/min. The temperature can be controlled by the amounts of vapor of liquid nitrogen with high pressure and electric heater, and it can be changed from –196°C to 300°C. The deviation of temperature is within about 0.5°C. Figs. 1.2(a) and 1.2(b) show DFMB and t/2-1/3PCCVN specimens set in the stage of the bend test machine, respectively. The scale of 0.5 mm distance was set in the back of specimen setting position. The adjustment of specimen position in the specimen stage is controlled by a small micrometer, which is set in the machine.

The position of the load cell can be measured by using a linear gauge (Mitutoyo, LGF sereies) and it is also controlled by a feed back control system for the position. The accuracy of the position for linear gauge is ±0.5 μm. The position of the specimen on the specimen stage equipped with a scale can be adjusted by using a small μ-meter instrument. The cross head is dropped gradually to the center of

specimen with V-notch. The displacement of the specimen is measured exactly by an optical probe (Keyence, LS-7030T) from the view port set in the chamber as shown in Fig. 1.1(b), and the accuracy for the displacement of the specimen is within ±0.15 μm.

Figs. 1.3(a) and 1.3(b) are load-displacement curves tested at 20°C in the DFMB and t/2-1/3PCCVN F82H-std specimens, respectively. The cross head of 0.1 mm/min was selected under the unloading compliance method. The fracture toughness tests for compact and three-point bend specimens was performed under the guidelines of the ASTM E 813 – 89 and E 1820 – 99a. Fracture toughness of DFMB and t/2PCCVN at RT was about 170 and 230 MPa $m^{1/2}$, respectively. These values were smaller than the value of 0.18DCT specimen as described in section of 1.3.2.

1.3.2 Fracture toughness testing of 0.18DCT

Fig. 1.4 shows the DCT test machine, which is manufactured to obtain fracture behavior for the 0.18DCT specimen. Fig. 1.4(c) shows the outboard gage attached to one of the disk compact specimen of F82H-std steel. This fracture toughness tests can be conducted in the temperature range from –180 to 300°C, and the temperature was controlled by the system of LN_2 vapor or electric heater. Tensile force, clip gauge displacement, cross head displacement and temperatures are measured and recorded during the tests. The load versus clip gage displacement curves are shown in Fig. 1.5. The displacement rate of the cross head was controlled at 0.2 mm/min under the unloading compliance method. Fracture toughness of F82H-std (low N) at RT was about 330 MPa $m^{1/2}$. This value is very similar to the value of previous study [9].

1.3. 3 Fracture Toughness Tests according to the ASTEM Standard E-1820-99a

Fracture toughness tests with several sizes of compact tension (CT) specimens are usually carried out according to the ASTM standard E 1820-99a. The notch direction in the CT specimens is fabricated to be parallel to the T-L orientation in the plate. Fatigue pre-cracking is induced to a ratio of pre-crack length to specimen width of about 0.4-0.5, followed by side-grooving by 20% of thickness. The unloading compliance method is applied for measuring the J-integral with a clip strain gage. The-integral value at cleavage instability, Jc, is converted to K_{JC} as follows:

$$K_{JC}^2 = J_C \cdot E/(1-\nu^2),$$

where E is the Young's modulus and = 0.29 is the Pission' ratio. The upper limit of valid is given by

$$K_{JC(limit)}^2 = Eb_o\sigma_{ys}/[M(1-\nu^2)],$$

where b_o is the ligament size, σ_{ys} is the yield stress at the testing temperature, and M is the constraint factor as defined to M = 30 in the ASTM E 1920. The measured K_{JC} for the small sized CT specimen, $K_{JC(small\ CT)}$,

is converted to the $K_{JC(1CT)}$, for the 1CT specimen as follows:

$$K_{JC(1CT)} = K_{min} + [K_{JC(small\ CT)} - K_{min}] (B_{small\ CT}/B_{1CT})^{1/b},$$

where $K_{min} = 2 \times 10^7$ Pa · $m^{1/2}$ is the minimum of K_{JC}, $B_{small\ CT}$ is gross thickness of tested small CT specimen, B_{1CT} is gross thickness of 1CT specimen and b = 4 is the shape parameter based on Weibull model. The median of $K_{JC(1CT)}$ is fitted by the MC curve identified by the reference temperature of To as follows:

$$K_{JC(medium)} = 30 + 70\exp[0.019(T - T_o)],$$

where T is the testing temperature. The cumulative probability for the failure is given by the Weibull model as follows:

$$P_f = 1 - \exp\{-[(K_{JC} - K_{min})/(K_o - K_{min})]^b\},$$

where K_o is the scale parameter.

1.4 Small Punch Testing

Small punch (SP) test machine was manufactured in a hot cell of the JMTR hot laboratory [10]. The SP test machine consists of a load controller, turntable with twelve specimen holders, a vacuum chamber and a furnace. The specimen holder consists of the upper and lower holders, a punch and a steel ball of 1mm diameter. A steel ball and a punch was pushed by the punch rod. The maximum load and stroke of the punch rod for the SP machine are 5 kN and 8 mm, respectively. The punch speed was controlled at 0.5 mm/min. SP energy was calculated from the area under the load-deflection curve up to the fracture load.

In this study, the F82H specimens of TEM disk type with 0.3 mm thickness were irradiated through F82H foil of 0.6 mm at about 120P°C with a beam of 100 MeV-He^{2+} particles by AVF cyclotron at TIARA (Takasaki Ion Accelerators for Advanced Radiation Application) facility of JAERI. The displacement damage was about 0.03 dpa and the stopping range of helium was about 1.25 mm. In this specimen, all helium atoms passed through the irradiated specimens. After the irradiation, the SP tests were performed in the JMTR (Japan Materials Testing Reactor) hot laboratory. The SP energy was calculated as a function of temperature as shown in Fig. 1.6. In this study, the change of DBTT due to displacement damage hardly occurred in this experiment and it was about 2-3°C. In the previous study [11] of 50 MeV-He^{2+} irradiation experiment, displacement damage in F82H steel was also about 0.03 dpa and the projected range of the helium ions controlled under an energy degrader was from 0 to 0.4 mm, and helium atoms were uniformly implanted to about 85 appm at about 100°C in the specimen with 0.3 mm in thickness. The shift of DBTT for the F82H steel implanted with 85 appm He was about 15°C [11]. The summaries of SP data tested at RT in F82H steel were given in Table 1.2. In the similar cyclotron helium implantation experiment of Kimura, it was reported that the shift of DBTT due to helium implantation of 120 appm was about 20°C in JLM-1 steel [12]. In our previous data, the ratio of the shift of DBTT to helium concentration in F82H steel was about 0.18°C/appmHe, and the ratio for Kimura data in JLM-1 steel was 0.22 °C/appmHe. These two data for the helium effect on DBTT in different martensitic steels were very similar. The DBTT obtained by the our previous SP experiments in F82H steel could be modified as 37.5°C for the DBTT measured using a 1/3CVN standard as determined from the correlation between SP data and 1/3CVN data [13]. The shift of DBTT due to displacement damage at 0.03 dpa can be evaluated from the other data of neutron irradiation experiment [14] and the value is estimated as about 5°C. In this experiment of F82H steel, the DBTT shift due to displacement damage of 0.03 dpa can be evaluated as about 6°C, and the value obtained by this study is very close to the result of the other study. Therefore, the shift of DBTT due to helium production of 85 appm could be concluded to be about 32°C in the 1/3CVN. In present study, the same result was obtained. On the other hands, in boron or nickel doping experiments of martensitic steels, similar results of the shift of DBTT due to helium production on the isotope-tailoring experiments were reported [14-15]. However, there was a possibility that the addition of boron or nickel may cause severe irradiation embrittlement. In this experiment, there are no effects of chemical additional element on DBTT [16-17], the shift of DBTT [11], the increment of irradiation hardening [18-19] and defect clusters [20-21] as reported in previous studies. It is therefore concluded that helium production can affect the shift of DBTT.

1.5 Charpy Impact Tests

Fig. 1.7 shows the dependence of Charpy impact energy on specimen size as a function of temperature, using t/2-CVN, 1/3CVN and t/2-1/3CVN specimens of F82H-std containing 20 ppm N (Low N). The upper shelf energy per cross section in fracture plane was decreasing with the reducing specimen size. The DBTT of t/2-CVN, 1/3CVN and t/2-1/3CVN was –82, -104 and –140°C, respectively. It is well known that DBTT depends strongly on the width of specimen, (B), and the length of ligament below the notch of the specimen, (b), [22-25]. The empirical correlations of DBTT of full size and sub-size specimens in reactor pressure vessel (RPV) steels were proposed:

$$DBTT_{full\ size} = DBTT_{sub\ size} + 98 - 15.1 \times \ln (Bb^2), \quad (1)$$

where $DBTT_{full\ size}$ and $DBTT_{sub\ size}$ are transition temperature for full size and sub-size Charpy impact specimens, respectively [22]. The values of DBTT, B and b in this study are given in Table 1.3, and the DBTT for 1/3CVN and t/2-1/3CVN can be estimated as about –130 and –141°C, respectively, by using eq. (1). The estimated value of DBTT for t/2-1/3CVN was good corresponds to the experimental data of F82H steel in this study, but the estimated value of DBTT for 1/3CVN was lower than the value of the present experimental data. The DBTT of F82H steel was lower than that of RPV steel, and the other factors such as the size and density of inclusions may be related to the correlations of DBTT for the size dependence. Further study is needed for the empirical correlations of DBTT of full size and sub-size specimens in RAF steels.

1.6 Summary

Small specimen test technology (SSTT) has been developed to investigate mechanical properties of nuclear materials. SSTT has been driven by limited availability of effective irradiation volumes in test reactors and accelerator-based neutron and charged particle sources. In this study new bend test machines have been developed to obtain fracture behaviors of F82H steel for very small bend specimens of pre-cracked t/2-1/3CVN (Charpy V-notch) with 20 mm-length and DFMB (deformation and fracture mini bend specimen) with 9 mm-length and disk compact tension of 0.18DCT type, and fracture behaviors were examined at 20°C. The effect of specimen size on DBTT (ductile-brittle transition temperature) of F82H steel was examined by using 1/2t-CVN, 1/3CVN and t/2-1/3CVN, and it was revealed that DBTT of t/2-1/3CVN and 1/3CVN was lower than that of t/2-CVN. DBTT behaviors due to helium and displacement damage in F82H-std irradiated at about 120°C by 50 or 100 MeV-He ions to 0.03 dpa were also measured by small punch tests.

1.7 References

[1] W.R. Corwin, G.E. Lucas (Eds.), The Use of Small-Scale Specimens for Irraidated Testing, ASTM-STP-888, American Society for Testing and Materials, Philadelphia, PA, 1986.

[2] W.R. Corwin, G.E. Lucas (Eds.), Small Specimens Test Techniques, ASTM-STP-1328, American Society for Testing and Materials, Philadelphia, PA, 1998.

[3] M. Sokolov, G.E. Lucas, J. Landes, 4P^{thP} Symposium on Small Specimen Test Techniques, STM-STP-1418, American Society for Testing and Materials, Philadelphia, PA, 2003.

[4] G.E. Lucas, "The development of small specimen mechanical test techniques", J. Nucl. Mater., 117 (1983) 327-339.

[5] P. Jung, A. Hishinuma, G.E. Lucas, H. Ullmaier, "Recommendation of miniaturized techniques for mechanical testing of fusion materials in an intense neutron source", J. Nucl. Mater., 232 (1996) 186-205.

[6] G.R. Odette, K. Edsinger, G.E. Lucas, E. Donahue, in: W.R. Corwin, S.T. Rosinski, E. van Walle (Eds.), Small Specimens Test Techniques, ASTM-STP-1328, American Society for Testing and Materials, Philadelphia, PA, 1998, pp. 298-321.

[7] G.R. Odette, "A cleavage toughness master curve model", J. Nucl. Mater., 283-287 (2000) 120-127.

[8] H. Matusi, IFMIF status and perspectives, presented at ICFRM-10.

[9] G.E. Lucas, G.R. Odette, K. Edsinger, B. Wirth and J.W. Sheckherd, "On the role of strain rate, size and notch acuity on toughness: a comparison of two martensitic stainless steels", ASTM STP 1270 (1996)790-814.

[10] T. Ishii, M. Ohmi, J. Saito, T. Hoshiya, N. Ooka, S. Jitsukawa and M. Eto, "Development of a small specimen test machine to evaluate irradiation embrittlement of fusion reactor materials", J. Nucl. Mater., 283-287 (2000) 1023-1027.

[11] E. Wakai, S. Jitsukawa, H. Tomita, K. Furuya, M. Sato, K. Oka, T. Tanaka, F. Takada, T. Yamamoto, Y. Kato, Y. Tayama, K. Shiba and S. Ohnuki, "Radiation hardening and -embrittlement due to He production in F82H steel irradiated at 250C in JMTR", J. Nucl. Mater., (2005), in press.

[12] A. Kimura, T. Morimura, R. Kasada, H. Matsui, A.Hasegawa and K. Abe, "Evaluation of ductile-brittle transition behavior of helium-implanted reduced activation 9Cr-2W martensitic steel by small punch tests", Effects of radiation on materials, STP1366, (2000)626-641.

[13] M. Eto, H. Takahashi, T. Misawa, M. Suzaki, Y. Nishiyama, K. Fukaya, S. Jitsukawa, "Development of a miniaturized bulge test (small punch test) for post-irradiation mechanical property evaluation", Small Specimen Test Techniques, ASTM STP 1204, (1993) 241-255.

[14] M. Rieth, B. Dafferener, H.-H. Rohrig, "Embrittlement behavior of different international low activation alloys after neutron irradiation", J. Nucl. Mater., 258 (1998) 1147-1152.

[15] K. Shiba, I. Ioka, J.P. Robertson, M. Suzuki, A. Hishinuma, "Mechanical properties of neutron irradiated F82H", Euromat-96, (1996) 265-272.

[16] E. Wakai, M. Sato, T. Sawai, K. Shiba, S. Jitsukawa, "Mechanical Properties and Microstructure of F82H Steel Doped with Boron or Boron and Nitrogen as a Function of Heat Treatment", Materials

Transactions 45 (2) , pp.407-410

[17] N. Okubo, E. Wakai. S. Matsukawa, K. Furuya, H. Tanigawa, S. Jitsukawa, "Heat treatment effects on microstructures and DBTT of F82H steel doped with and nitrogen", Materials Transactions, JIM, 46(2), pp.193-195.

[18] E. Wakai, S. Matsukawa, T. Yamamoto, Y. Kato, F. Takada, M. Sugimoto, S. Jitsukawa, "Mechanical property of F82H steel doped with boron and nitrogen", Materials Transactions 45 (8) , pp.2641-2643.

[19] E. Wakai, T. Taguchi, T. Yamamoto, H. Tomita, F. Takada, S. Jitsukawa, "Effects of helium production and heat treatment on neutron irradiation hardening of F82H steels irradiated with neutrons", Materials Transactions, JIM, 46(3), pp.481-486.

[20] E. Wakai, Y. Miwa, N. Hashimoto, J.P. Robertson, R.L. Klueh, K. Shiba, K. Abiko, S. Furuno, S. Jitsukawa, "Microstructural study of irradiated isotopically tailored F82H steel", J. Nucl. Mater., 307-311 (2002)203-211.

[21] E. Wakai, N. Hashimoto, Y. Miwa, J.P. Robertson, R.L. Klueh, K. Shiba, S. Jitsukawa, "Effect of helium production on swelling of F82H irradiated in HFIR", J. Nucl. Mater., 283-287(2000)799-805.

[21] M.A. Sokolov, R.K. Nastad, "On impact testing of subsize Charpy V-notch type specimens", ASTM STP 1270 (1996)384-414.

[22] H. Kayano, H. Kurishita, A. Kimura, M. Narui, M. Yamazaki, Y. Suzuki, "Charpy impact testing using miniature specimens and its application to the study of irradiation behavior of low-activation ferritic steels", J. Nucl. Mater., 179(1991)425-428.

[23] H. Kurishita, T. Yamamoto, M. Narui, H. Suwarno, T. Yoshitake, Y. Yano, M. Yamazaki, "Specimen size effects on ductile-brittle transition temperature in Charpy impact testing", J. Nucl. Mater., 329-333(2004)1107-1112.

[24] H. Kurishita, H. Kayano, M. Narui, M. Yamazaki, Y. Kano and I. Shibahara, "Effects of V-notch dimensions on Charpy impact test results for differently sized miniature specimens of ferritic steel", Mater. Trans., JIM, 34(1993)1042-1052.

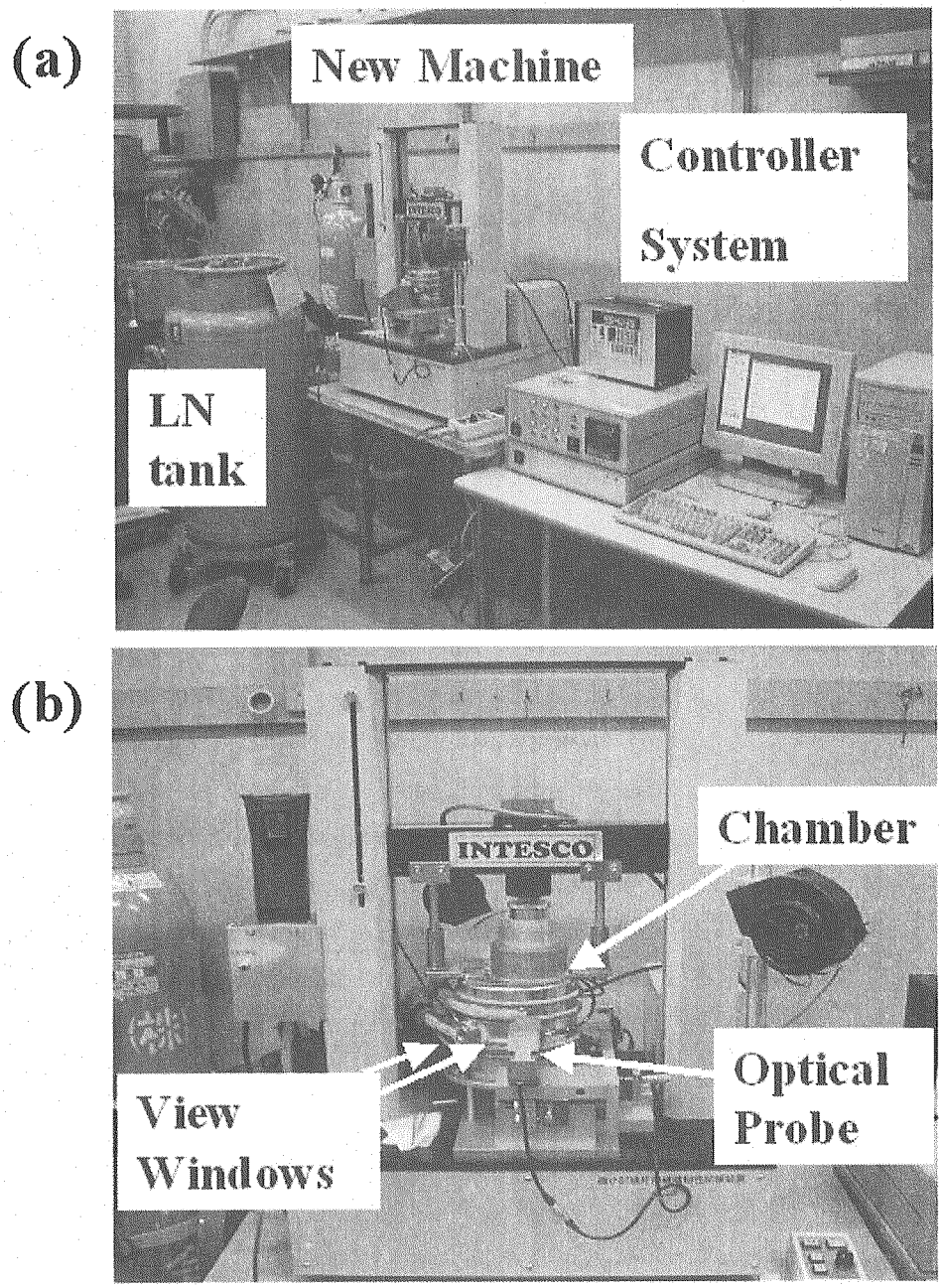

Fig. 1.1 A new bend test machine, which is manufactured to obtain fracture behavior for very small bend specimens of pre-cracked 1/3CVN with 20 mm-length and DFMB with 9 mm-length. (a) Configuration of the machine and (b) Chamber and the optical probe.

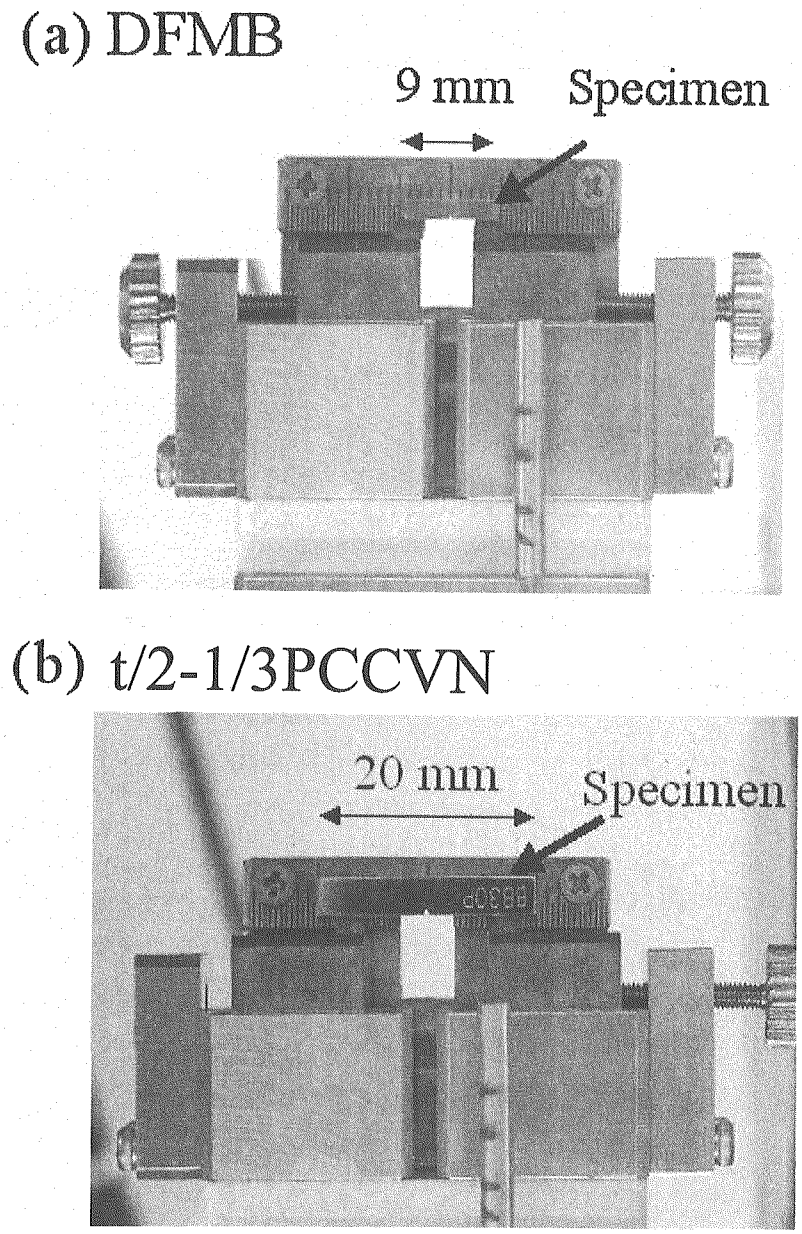

Fig. 1.2 DFMB specimen and (b) t/2-1/3PCCVN specimen of F82H-std (low N) set in the stage.

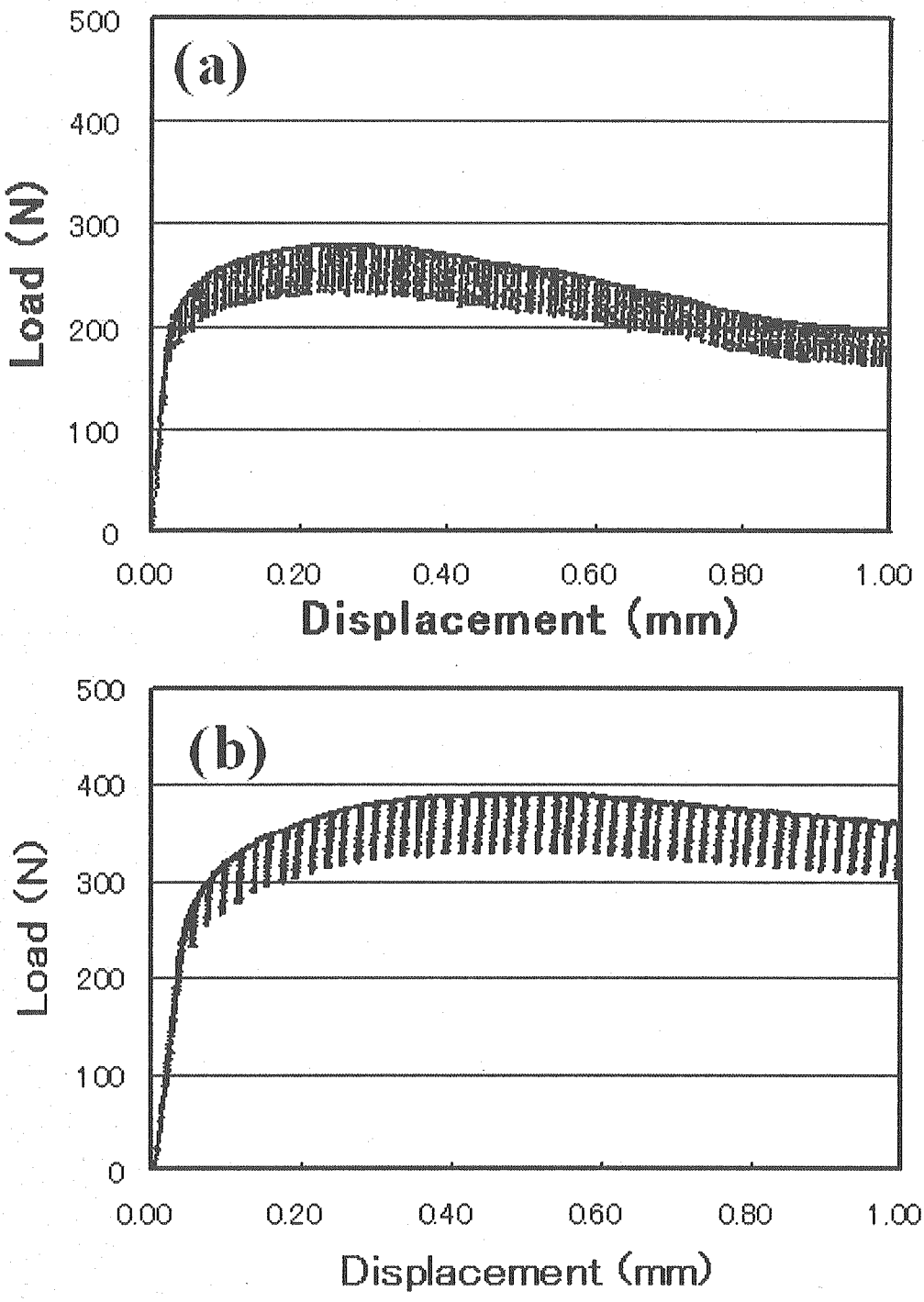

Fig. 1.3 Load and displacement curves obtained from (a) DFMB and (b) pre-cracked t/2-1/3CVN specimens of F82H-std (low N).

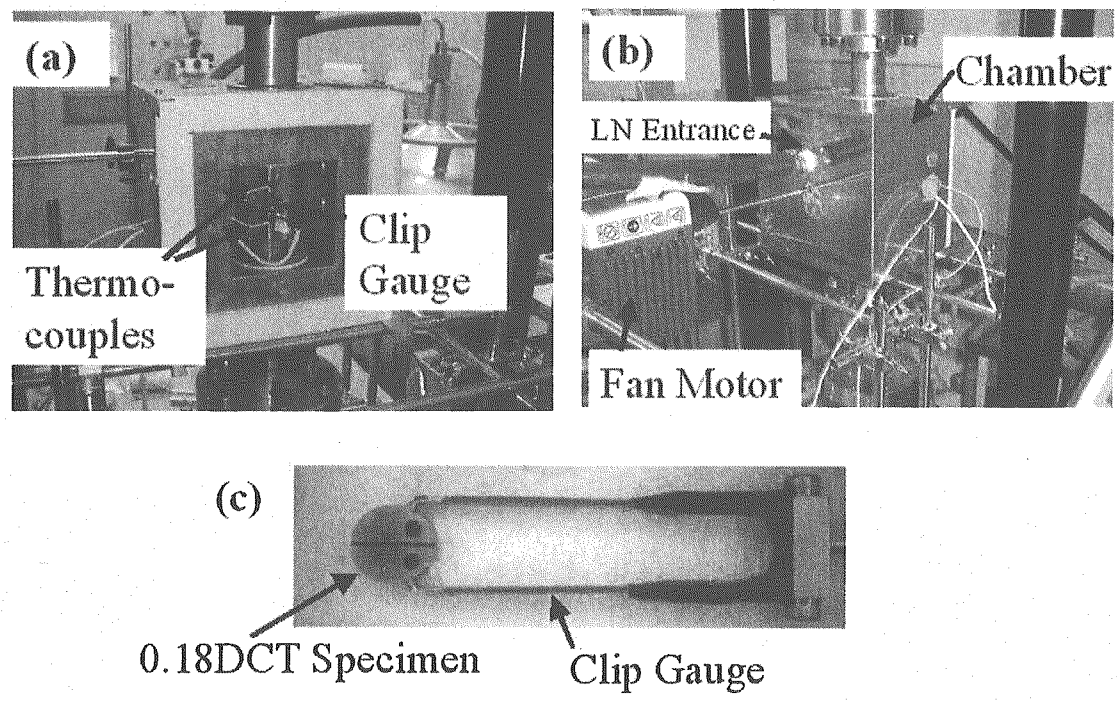

Fig. 1.4 0.18DCT machine, (a) chamber inside, (b) front of Chamber and (c) clip gauge and specimen.

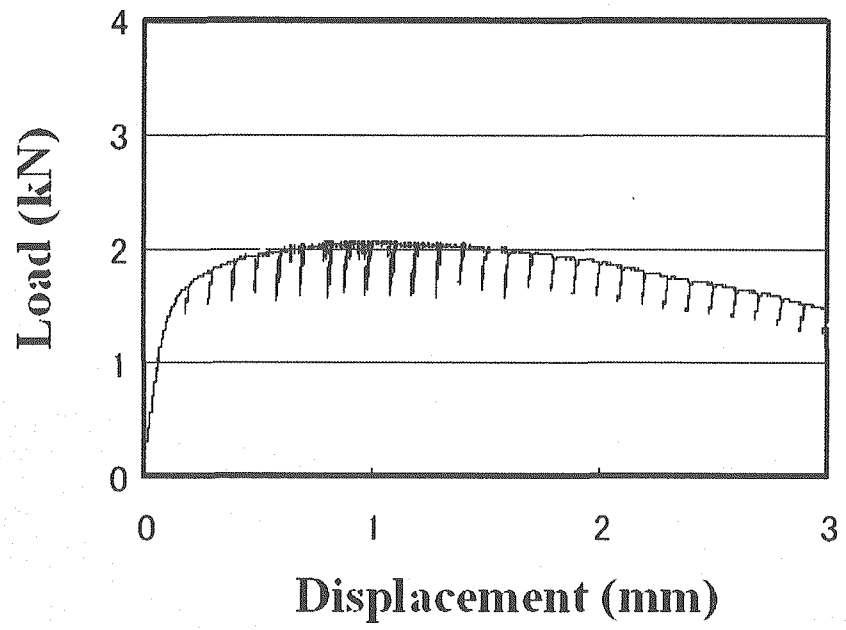

Fig. 1.5 Load and displacement curves obtained from (a) DFMB specimen and (b) t/2-1/3PCCVN of F82H-std (low N).

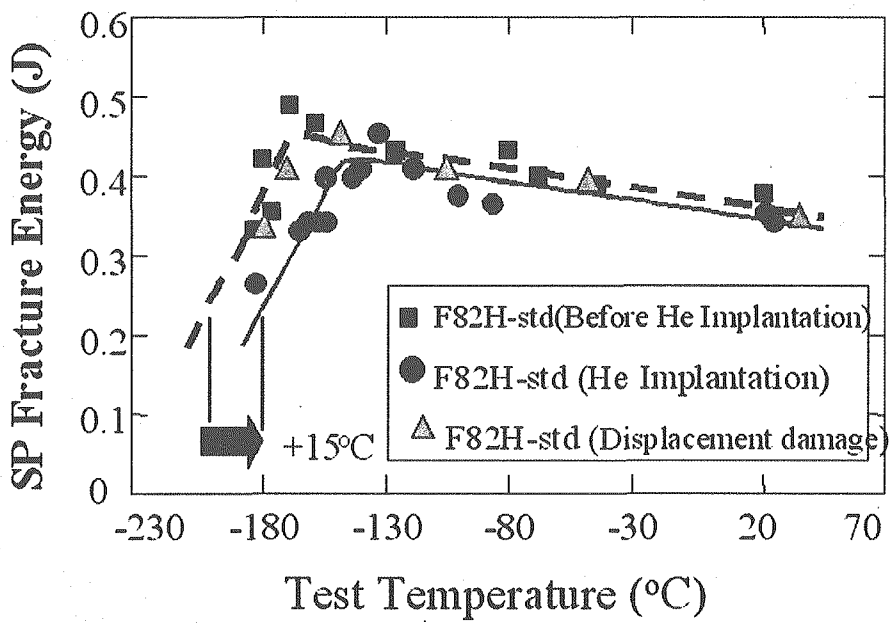

Fig. 1.6 SP energy as a function of temperature in F82H-std (IEA).

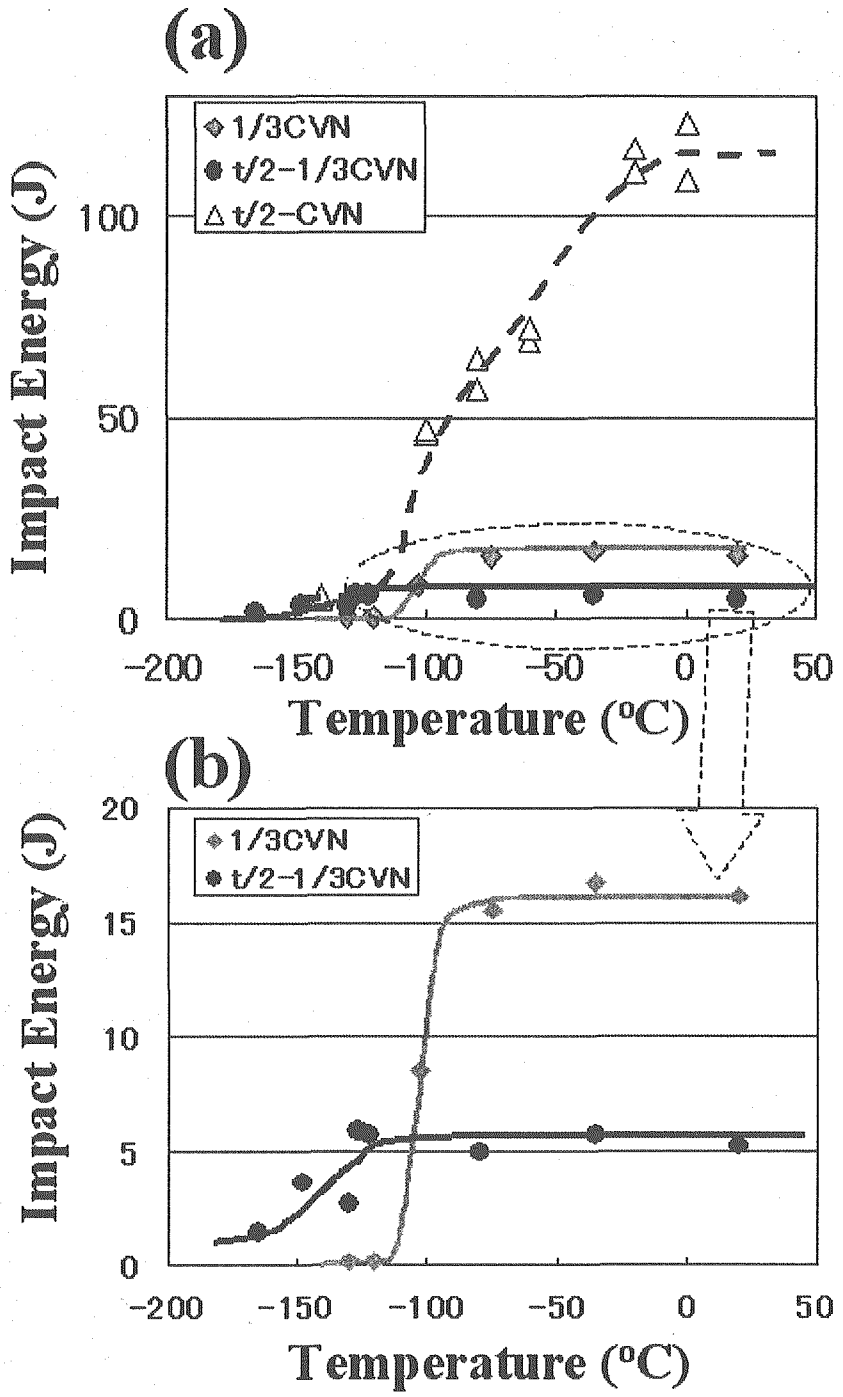

Fig. 1.7 Dependence of specimen size on Charpy impact energy as a function of temperature, using t/2-CVN, 1/3CVN and t/2-1/3CVN specimens of F82H-std (Low N).

Table 1.1: Chemical compositions of the specimens used in this study (wt%)

Materials	N	C	Si	Mn	P	S	Cr	W	V	Ta
F82H-std (IEA)	0.007	0.09	0.07	0.10	0.003	0.001	7.82	1.98	0.19	0.04
F82H-std (Low N)	0.0023	0.099	0.11	0.10	0.007	0.001	7.92	1.97	0.18	0.05

Table 1.2: SP-yield load, SP-maximum load, cracking load, deflection at a maximum of load and total elongation of F82H steels tested at RT by SP

	Displacement damage (dpa)	He (appm)	Yield Load (N)	Maximum Load (N)	Cracking Load (N)	Deflection at P_{max} (mm)	Total Deflection (mm)
F82H	0	0	123	522	348	0.38	0.78
F82H(50MeV-He)	0.03	85	120	493	337	0.38	0.75
F82H(100MeV-He)	0.03	0	123	499	350	0.48	0.74

Table 1.3: DBTT, width of specimen, (B), and the length of ligament below the notch, (b), of F82H steel for t/2-CVN, 1/3CVN and t/2-1/3CVN Charpy impact specimens. The estimation of DBTT in t/2-CVN, 1/3CVN and CVN was calculated by using a data of t/2-CVN.

	Full size or Sub size	B (mm)	b (mm)	DBTT (°C) (Experimental data)	DBTT (°C) (Estimation)
t/2-CVN	Subsize	5	8	-82	(-82)
1/3CVN	Subsize	3.3	2.79	-104	-130
t/2-1/3CVN	Subsize	1.65	2.79	-140	-141
CVN	Full-size	10	8	-	-81.6

2. Mechanical Property of F82H Steel Doped with Boron and Nitrogen

2.1 Research Background and The purpose of This Study

Reduced-activation ferritic/martensitic steels are candidate materials for the blanket structure of fusion reactors. The structure materials must not only withstand radiation damage, but also accommodate helium atoms due to transmutation process. The effects of neutron irradiation on tensile deformation, DBTT, and microstructures of F82H and the other ferritic/martensitic steels were reported[1-6]. Radiation hardening occurred mainly at irradiation temperatures lower than about 400° C, and it increased with decreasing irradiation temperature up to about 250° C. The issue of helium accumulation on mechanical properties has been an ongoing concern. Recently, the effect of helium production on radiation hardening has been examining and the large enhancement of hardening due to helium from 600 appm to 10000 appm is detected in the tensile testing for 9Cr martensitic steels EM10 and T91 implanted by cyclotron experiments[7]. Small enhancements of radiation hardening are also reported in neutron irradiation experiment[8,9] and ion beam experiments[10]. In order to examine the quantified analysis for the dependence of helium production on hardening, isotope ^{10}B dope technique to produce He atom in the alloys with a different ^{10}B concentration is effective method under a mixed spectrum reactor irradiation with thermal and first neutrons. Doping of B element can affect on mechanical properties before and after irradiation, and the errors induced from the effect of B on mechanical properties have to be minimized by comparing the results for the mechanical testing of ^{10}B and ^{11}B doped specimens. The first purpose of this study is focused to evaluate quantitatively the contribution of helium production on hardening and fracture behavior in F82H irradiated at 300°C for the synergistic effect of helium and displacement damage.

Effect of heat treatment on mechanical properties of Fe-8Cr-2W-0.1C-0.2V-0.04Ta martensitic steel F82H doped with about 60 mass ppm B or both of 60 mass ppm B and 200 mass ppm N was examined, and the F82H doped with boron and nitrogen had an excellent mechanical[11]. The second purpose of the present study is to examine the effect of specimen size on tensile properties and DBTT in F82H doped with boron and nitrogen.

2.2 Experimental Procedure

The materials used in this study and the compositions are given in Table 2.1. In order to produce helium atoms the materials were doped with about 60 mass ppm ^{10}B. The purity of isotope elements of ^{10}B and ^{11}B used in this study was about 95%. The plates of these materials with about 15 mm thickness were normalized at 1040°C for 40 minutes and tempered at 750° C for 60 minutes. The SS-3 tensile specimens were 0.76 mm thick with a gage length of 7.62 mm and 1.55 mm in width. Irradiation was carried out at nominally 250°C in the capsule 00M-66A of the Japan Materials Test Reactor (JMTR) in the Japan Atomic Energy Research Institute (JAERI) to neutron fluences of 1.4 x 10^{21} n/cm^2 (E >1 MeV) and 1.2 x 10^{21} n/cm^2 (E <0.683 eV), resulting in a displacement damage of ~2.2 dpa. The averaged displacement damage induced by the reaction of $^{10}B(n, \alpha)^7Li$ was calculated as about 0.2 and 0.1 dpa for the F82H+^{10}B and F82H+^{11}B+^{10}B, respectively. The total displacement damage due to the transmutation reaction and neutron irradiation was 2.4 dpa in the F82H+^{10}B.

After the neutron irradiation, tensile testing was carried out in vacuum at a strain rate of 4 x 10^{-4} s^{-1} at 25°C in a hot cell of the JMTR hot laboratory. After the tests, the fracture surface was observed by a scanning electron microscope (SEM). The concentrations of helium in the specimens after the irradiations were measured by using a mass analyzer of magnetic reflection type[22]. The helium concentrations produced from a reaction of $^{10}B(n, \alpha)^7Li$ in the F82H+B steels irradiated in the JMTR were evaluated and the helium concentrations produced in the F82H-std, F82H+^{10}B, F82H+^{11}B and F82H+^{10}B+^{11}B steels were 5, 331, 14 and 194 appm, respectively.

The effect of specimen size on mechanical properties was examined for a F82H doped with about 60 mass ppm B and 200 mass ppm N. The detail preparations of this alloy were reported[23]. In tensile testing, JIS 14A tensile specimen (6 mm diameter and 33 mm length in the gauge region) and SS-J3 (small size Japanese-3, 0.76 mm thick with a gage length of 7.62 mm and 1.55 mm in width) were measured at room temperature under a strain rate of 2.5 x 10^{-3} and 4.4 x 10^{-4} s^{-1}, respectively. The ductile-brittle transition temperatures of the specimens were measured by using half-size Charpy impact specimens (5 mm width, 10 mm height, 50 mm length) with V-notch and smaller size impact specimens (1.65 mm width, 3.3 mm height, 18 mm length).

2.3 Mechanical Properties of F82H and F82H Doped With Boron

2.3.1 Tensile Testing After Neutron Irradiation

The stress-strain curves of F82H, F82H+^{10}B, F82H+^{11}B, and F82H+^{10}B+^{11}B steels irradiated at 300°C in JMTR were given in Fig. 2.1. The tensile properties were measured at 25°C. The increments of yield stress, ΔYS, and ultimate tensile strength, ΔUTS, due to irradiation are given in Fig. 2.2. In the F82H+^{10}B+^{11}B and F82H+^{10}B, the ΔYS and ΔUTS increased somewhat with increasing helium production. In Fig. 2.3, the fracture surfaces of tensile specimens are shown, and the reduction area decreased in the F82H+^{10}B. The ratio of fracture strength to fracture area in tensile testing was given in Fig. 2.4, and the approximate fracture stress decreased in the F82H+^{10}B+^{11}B and F82H+^{10}B. This result might indicate that the fracture stress was reduced by a high amount of helium production. ΔYS due to helium production, ΔYS(He), is defined as the difference between ΔYS of F82H+^{10}B or F82H+^{10}B+^{11}B and ΔYS of F82H+^{11}B and it is given by

$$\Delta YS(He) = \Delta YS(F82H+^{10}B \text{ or } F82H+^{10}B+^{11}B) - \Delta YS(F82H+^{11}B), \quad (1)$$

$$\Delta YS(F82H+^{10}B) = YS(F82H+^{10}B)_{irrad.} - YS(F82H+^{10}B)_{non\text{-}irrad.}, \quad (2)$$

where $YS_{irrad.}$ and $YS_{non\text{-}irrad.}$ are the yield stress of the specimen after and before irradiation, ΔYS induced by helium production is detected at around 330 appmHe. The radiation hardening due to helium production was also reported in T91 martensitic steel implanted with helium[14,15], and the formation of cavities was observed. It could be expected that the cavities would be also formed in this experiment, and the factor of hardening due to helium was caused by the formation of cavities.

2.3.2 Effect of Specimen Size on Mechanical Properties

The dependence of specimen size on the DBTT was examined as shown in Fig. 2.5. The DBTT of the standard size and small specimens were –83°C and –95°C, respectively. There was a difference about 12°C between these data. In the tensile testing, similar values for YS, UTS and TE were obtained in the different size specimens as given in Fig. 2.6. In Figs. 2.7(a) and (b), tensile properties of F82H doped with boron and nitrogen were shown as a function of temperature. The properties of F82H doped with boron and nitrogen were very similar to those of F82H tested at 25°C.

2.4 Summary

Dependence of fracture properties and hardening was examined as a function of helium production in tensile specimens of a martensitic steel F82H (Fe-8Cr-2W-0.1C-0.04Ta) irradiated at 300°C to 2.3 dpa by neutron irradiation in the JMTR (Japan Materials Testing Reactor). The specimens used in this study were F82H, F82H+60ppm^{11}B, F82H+30ppm(^{11}B+^{10}B) and F82H+60ppm^{10}B. The helium range produced from ^{10}B(n, α)^{7}Li reaction was from 5 to 330 appm in the specimens. The tensile testing was performed at 25°C. The radiation hardening due to helium production was detected at 330 appmHe. The degradation of fracture stress due to helium production was approximately evaluated from the fracture strength and the reduction area.

Effect of specimen size on tensile and Charpy impact properties in F82H doped with 60 ppm boron and 200 ppm nitrogen was also examined. The JIS 14A and SS-J3 (Small Size – Japanese-3 type) were used for the tensile specimens, and half size (55 mm in length, 10 mm in height and 5 mm in width) and 0.5-1/3CVN (18mm in length, 3.3 mm in height and 1.65 mm in width) were used for the Charpy impact testing. The tensile properties were a similar to each other. However, the ductile-brittle transition temperature measured in smaller size specimen was somewhat lower than that in the standard size specimen.

2.5 References

1) R. L. Klueh, M.A. Sokolov, K. Shiba, Y. Miwa and J.P. Robertson: J. Nucl. Mater., **283-287**(2000)478-482.
2) E. Wakai, A. Hishinuma, K. Usami, Y. Kato, S. Takaki and K. Abiko: Mater. Trans., JIM, vol.**41**, No.9, (2000)1180-1183.
3) E. Wakai, A. Hishinuma, T. Sawai, S. Kato, S. Isozaki, S. Takaki and K. Abiko: Phys. Stat. Sol. (a), **160**(1997)441-448.
4) A.F. Rowcliffe, J.P. Robertson, R.L. Klueh, K. Shiba, D.J. Alexander, M.L. Grossbeck, S. Jitsukawa: J. Nucl. Mater. **258**(1998)1275-1279.
5) E.I. Materna-Morris, M. Rieth and K. Ehrlich: Effects of radiation on materials, STP**1366**, (2000)597-611.
6) M. Rieth, B. Dafferner and H.-D. Rohrig: J. Nucl. Mater. **258**(1998)1147-1152.
7) J. Henry, M.-H. Mathon and P. Jung: J. Nucl. Mater., **318**(2003)249-259.
8) R.L. Klueh and J.M. Vitek: J. Nucl. Mater., **150**(1987)272-280.
9) L.K. Mansur and M.L. Grossbeck, J. Nucl. Mater., **155-157**(1988)130-147.
10) M. Ando, E. Wakai, H. Tanigawa, T. Sawai, K. Furuya, S. Jitsukawa, H. Takeuchi, K. Oka, S. Ohnuki and A. Kohyama: J. Nucl. Mater., (2004), in press.
11) E. Wakai, M. Sato, T. Sawai, K. Shiba and S. Jitsukawa: Mater. Trans. Vol. **45**, No. 2(2004)407-410.

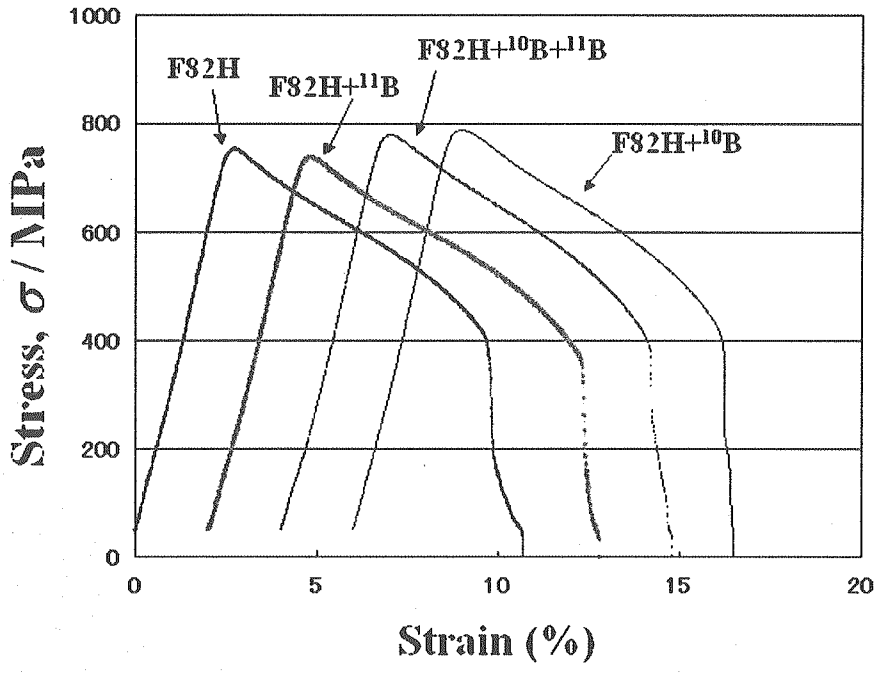

Fig. 2.1 Tensile curves of F82H, F82H+60ppm^{11}B, F82H+30ppm(^{10}B+^{11}B) and F82H+60ppm^{10}B steels irradiated at 300°C to 2.3 dpa in JMTR. The tensile testing was performed at 25°C under a strain rate of 4.4×10^{-4} s^{-1}.

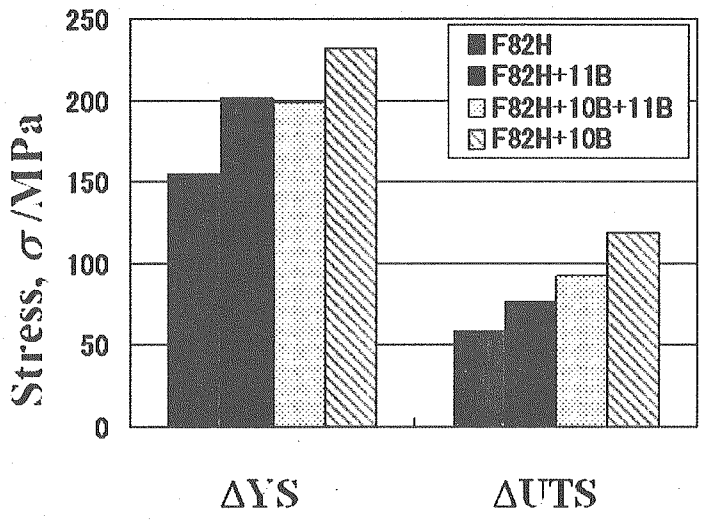

Fig. 2.2 Radiation hardening of yield stress (YS) and ultimate tensile stress (UTS) due to irradiation in the F82H, F82H+60ppm^{11}B, F82H+30ppm(^{10}B+^{11}B) and F82H+60ppm^{10}B steels.

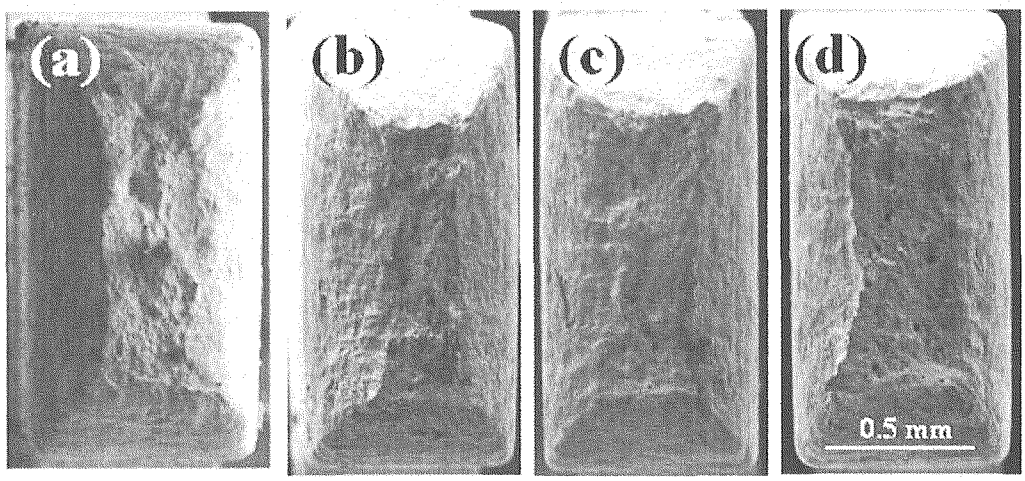

Fig. 2.3 Fracture surfaces of (a) F82H, (b) F82H+60ppm^{11}B, (c) F82H+30ppm(^{10}B+^{11}B) and (d) F82H+60ppm^{10}B steels after the tensile testing.

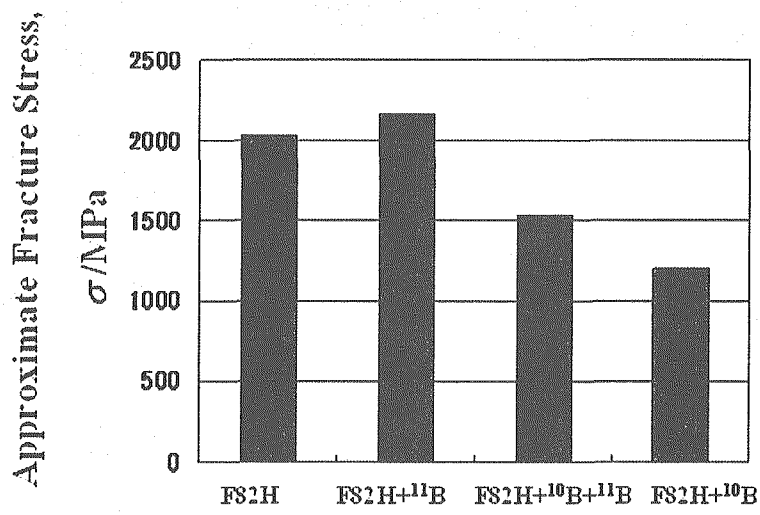

Fig. 2.4 Approximate fracture stress evaluated from the relation between fracture strength and reduction area.

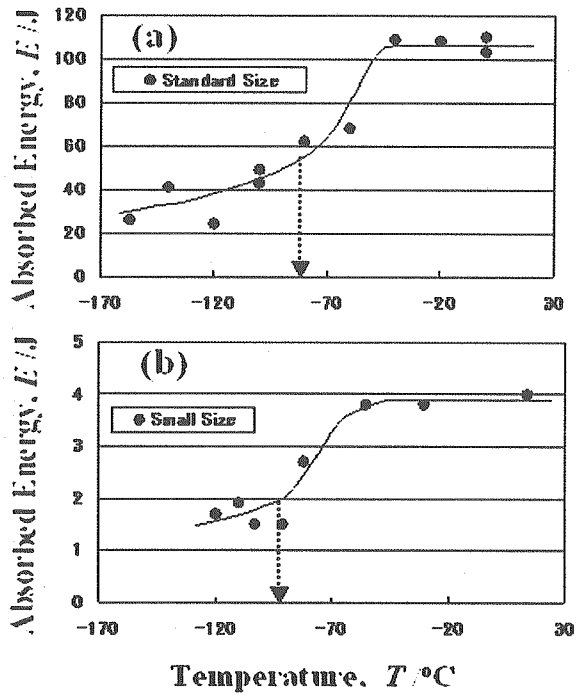

Fig. 2.5 Ductile-brittle transition temperatures in F82H+60ppmB+200ppmN steel obtained from standard size and small size impact specimens.

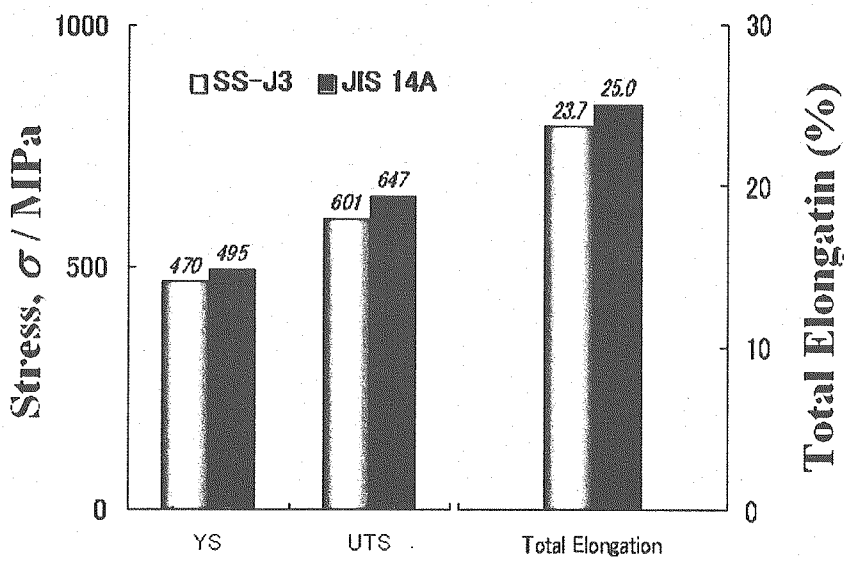

Fig. 2.6 Yield stress, ultimate tensile stress and total elongations of F82H+60ppmB+200ppmN steel obtained from a standard size (JIS 14A) and a small size (SS-J3) specimens.

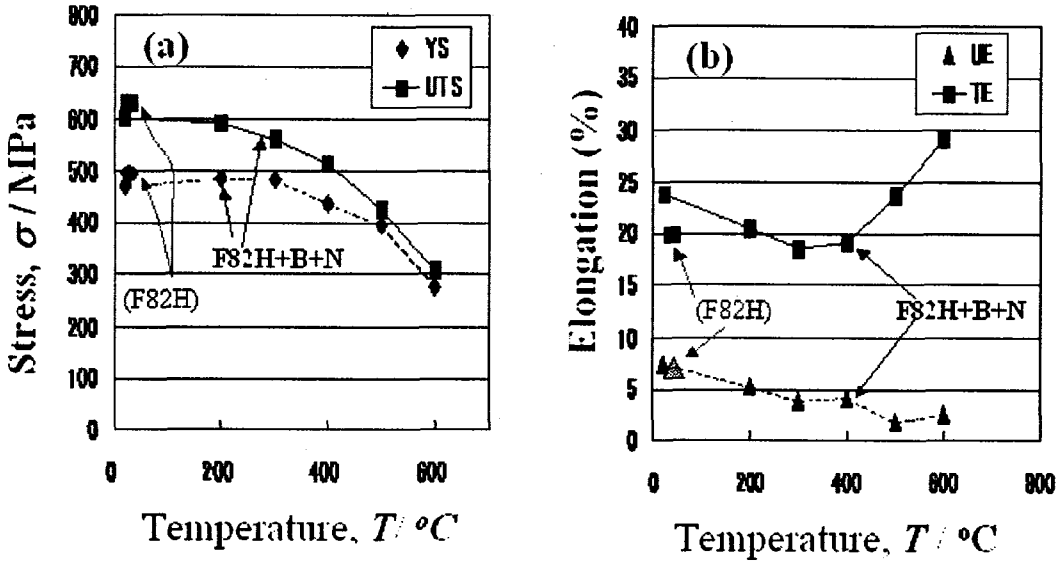

Fig. 2.7 Tensile property of F82H+60ppmB+200ppmN steel.

Table 2.1: Chemical compositions of materials (mass %)

Materials	B	N	C	Si	Mn	P	S	Cr	W	V	Ta
F82H	0.0003	0.0028	0.099	0.11	0.10	0.007	0.001	7.92	1.97	0.18	0.05
F82H+^{10}B	0.0061	0.0022	0.097	0.10	0.10	0.007	0.001	7.96	1.98	0.18	0.05
F82H+^{11}B	0.0059	0.0011	0.093	0.11	0.10	0.007	0.001	8.02	1.98	0.18	0.05
F82H+^{10}B+^{11}B	0.0067	0.0020	0.094	0.12	0.90	0.007	0.001	8.01	2.01	0.18	0.05
F82H+B+N	0.0059	0.0190	0.099	0.099	0.10	0.006	0.001	8.09	2.10	0.30	0.039

3. Effect of Gas atoms and Displacement Damage on Mechanical Properties and Microstructures of F82H

3.1 Research Background and The Purpose of This Study

Ferritic/martenisitc steels are one of candidate materials for the vessel of spallation target [1], and reduced-activation ferritic/martenistic (RAF) steels are first priority materials of structure for fusion nuclear reactors [2]. In these systems, particles with high energy are irradiated to the vessels or the structures, and helium and hydrogen atoms are generated in materials. These systems are desired to operate at relatively higher temperatures. It is reported that helium atoms can affect on DBTT [3-7], swelling behavior [8-15] and irradiation hardening [16-23] in martensitic steels.

In studies of synergistic effects of displacement damage and helium on mechanical properties and microstructure, there are some experimental methods. The synergistic effect can be examined by high energy proton beams to target materials such as SINQ (Swiss Spallation Neutron Source) [24] and LANSCE (Los Alamos Neutron Science Center) [25]; Reactor neutron irradiation can be partially simulated by martensitic steels doped with ^{10}B or ^{58}Ni in a mixed spectrum fission reactor [12, 26-28]; A multi-ion irradiation experiment is also very important method to control of helium production ratio during irradiation [8-9,11,17]. Particularly, this method produces fusion relevant high-energy cascades at controllable helium production (He/dpa). Moreover, the effects of helium on radiation hardening behavior can be evaluated by combining ion-irradiation experiments and an ultra micro-indentation technique [16-17]. The effects of helium atoms on mechanical properties and microstructures were also examined by the cyclotron helium implantation [3,19,29-31], and hardness changes, DBTT shift, fracture behaviors and creep strength [30-31] of martensitic steels due to helium were investigated.

In this study, the dependence of irradiation temperature and gas atoms on swelling, irradiation hardening and DBTT shift due to gas atoms in martensitic F82H steel have been examined by some experimental methods such as multiple ion beams, cyclotron helium implantation and neutron irradiation of a reactor.

3.2 Experimental Procedure

3.2.1 Multiple Ion Beam Experiments of Hardness and Microstructures

The chemical compositions of F82H-std steel used in this study are given in Table 2.1. The heat treatment of F82H steel were first normalized at 1040°C for 38 min and tempered at 750°C for 1 h. The material was cut to small coupon type specimens (6 × 2 × 0.8 mm^3). One of the 6 × 0.8 mm sides was irradiated after polishing with SiC paper #4000 and 0.3 μm alumina powder and finally to an electrolytic surface polishing. The ion-beam irradiation experiment was carried out at the TIARA facility in JAERI. The configuration of the beam lines and specimens is shown in Fig. 3.1. The specimens were irradiated at 270, 360 and 430°C. Single irradiation was performed with 10.5 MeV-Fe^{3+} ions. Dual irradiation was also performed with simultaneous beams of 10.5 MeV-Fe^{3+} and 1.05 MeV-He^{+} ions using an energy degrader for helium ions. Triple irradiation was done with simultaneous beams of 10.5 MeV-Fe^{3+}, 1.05 MeV-He^{+} and 0.38 MeV-H^{+} ions using energy degraders for helium and hydrogen atoms. Helium and hydrogen implantations were performed using an aluminum foil energy degraders in order to control the helium and hydrogen distributions in the depth range of about 0.8–1.3 μm from the specimen surface. The irradiation was performed to 20–50 dpa at the depth of 1.0 μm from the irradiation surface. The damage rate was about 1.0×10^{-3} dpa/s. The ratios of helium and hydrogen to dpa were about 10 appmHe/dpa and 40 appmH/dpa, respectively. The irradiated specimens were then indentation-tested at a load range of 10–25 mN using an UMIS-2000 (CSIRO, Australia) ultra micro-indentation testing system. The direction of indentation was chosen to be parallel to the ion beam axis or normal to the irradiated surface. The shape of the indenter tip was a Berkovich tip. The micro-indentation results were analyzed in the manner outlined by Oliver and Pharr [32]. Micro-indentation tests were performed at loads to penetrate about 0.40 μm in this study as shown in Fig. 3.2. TEM foils of the ion-irradiated specimens were made by using a Hitachi FB-2000A focused ion beam (FIB) processing instrument with micro-sampling system operated at 30 kV by Ga^{+} ions at the Tokai Hot Laboratory and a low energy Ar ion gun operated at 1 kV and 0.2 kV. The microstructural examination was carried out using a Hitachi-HF-2000 transmission electron microscope (TEM) operated at 200 kV.

3.2.2 Cyclotron Helium Implantation Experiment and Small Punch Test for 3 mmϕ Disk

The TEM disk specimens of F82H-std steel with 0.3 mm thickness were implanted at about 120°C with a beam of 50 MeV-He^{2+} particles by AVF cyclotron at TIARA facility of JAERI. An energy degrader was used to implant helium into the specimens from top to bottom uniformly [33]. The concentration of the He and displacement damage in the specimen implanted by cyclotron irradiation was evaluated as about 85 appm He and 0.03 dpa, respectively. After the helium implantation experiment, SP experiment and TEM observations were performed. The effect of helium production on fracture behavior at 20, 600 and 700°C was examined by small punch (SP) tests. The fracture surfaces were observed by a scanning electron

microscope (SEM) after the SP. The SP test was graphically shown in Fig. 3.3.

3.2.3 Neutron Irradiation of Tensile and Fracture Toughness Specimens

The materials used in this study and the compositions are also given in Table 3.1. In order to produce helium atoms the materials were doped with about 60 mass ppm ^{10}B. The purity of isotope elements of ^{10}B and ^{11}B used in this study was about 95%. The plates of these materials with about 15 mm thickness were normalized at 1040°C for 40 minutes and tempered at 750° C for 60 minutes. 0.18DCT and SS-3 specimens were used to evaluate fracture behavior and hardening in this study. The 0.18DCT specimens (12.5 mm diameter and 4.63 mm thickness) were machined in the T-L orientation so that crack propagation occurred parallel to the rolling direction. Fatigue pre-cracking was performed at room temperature in a condition of crack length to specimen width ratio (a/W) of approximately 0.46. This was followed by side-grooving on each side to depth of ~10% of specimen thickness. The SS-3 tensile specimens were 0.76 mm thick with a gage length of 7.62 mm and 1.55 mm in width. Irradiation was carried out at nominally 300°C in the capsule 00M-65A of the Japan Materials Test Reactor (JMTR) in the Japan Atomic Energy Research Institute (JAERI) to neutron fluences of 1.4 x 10^{21} n/cm^2 (E >1 MeV) and 1.2 x 10^{21} n/cm^2 (E <0.683 eV), resulting in a displacement damage of ~2.2 dpa. The averaged displacement damage induced by the reaction of $^{10}B(n, \alpha)^7Li$ was calculated as about 0.2 and 0.1 dpa for the F82H+^{10}B and F82H+^{11}B+^{10}B, respectively. The total displacement damage due to the transmutation reaction and neutron irradiation was 2.4 dpa in the F82H+^{10}B. After the neutron irradiation, tensile testing was carried out in vacuum at a strain rate of 4 x 10^{-4} s^{-1} at 25°C and fracture toughness testing was also performed in a hot cell of the JMTR hot laboratory. After theses tests, the fracture surface was observed by a scanning electron microscope (SEM). The concentrations of helium in the specimens after the irradiations were measured by using a mass analyzer of magnetic reflection type [3]. The helium concentrations produced from a reaction of $^{10}B(n, \alpha)^7Li$ in the F82H+B steels irradiated in the JMTR were evaluated and the helium concentrations produced in the F82H+^{10}B, F82H+^{11}B and F82H+^{10}B+^{11}B steels were about 330, 14 and 190 appm, respectively.

3.3 Irradiation Effects

3.3.1 Irradiation Hardening by Ion Irradiations

Fig. 3.4 shows the dose dependence of irradiation hardening at 360°C up to 50 dpa in F82H martensitic steel. The micro-hardness of F82H steel rapidly increased up to 20 dpa and it tended to saturate from 20 dpa to 50 dpa. The hardness of F82H irradiated with triple beams was slightly higher than the others, and the hardness of F82H irradiated with dual beams was slightly higher than the single irradiation. The difference of hardness of F82H steel irradiated to 50 dpa between single irradiation and multiple irradiations was smaller than that to 20 dpa. The enhancements of hardness due to the multiple irradiations are indicated that the implanted helium and hydrogen atoms in martensitic steel can affect on irradiation hardening at 360°C. According to Ando et al, irradiation hardening could be enhanced by the ratio of helium implantation to displacement damage and total amount helium concentration, and the enhancement of hardening was related to the formation of cavities [16]. Similar result for the enhancement of irradiation hardening due to high amounts of helium atoms was reported [19].

Fig. 3.5 shows the hardness changes of F82H steel irradiated at 270 and 360°C to 20 dpa under single, dual and triple irradiations. Radiation hardening for single irradiation, dual irradiation and triple irradiation was very similar to each other, and the results were different from those at 360°C to 20 dpa. Radiation hardening due to single irradiation in F82H steel irradiated at 270°C was comparable to that due to single irradiation at 360°C, while the irradiation hardening due to multiple irradiations at 270°C was smaller than that at 360°C. The difference of beam conditions for the changes of irradiation hardening was not detected at 270°C. In the different heat treatment specimens, the irradiation hardening in the first N&T (normalizing and tempering) heat specimens was slightly larger than the others of the second heat treatment, and the radiation hardening was reduced by the re-heat treatment. The cause of the hardening changes induced by the re-heat treatment may be related to changes of the homogeneity level of matrix. A similar result of the re-heat treatment effect was reported by neutron irradiation [23,34-35]. In this experiment, it is found that the effect of heat treatment on irradiation hardening is also valid for the dual and triple irradiations.

3.3.2 Swelling Behavior under Ion Irradiations

In previous study [8-9], swelling behavior of F82H steel was examined at temperatures of 470, 510 and 600°C to 50 dpa under dual ion beams of about 15 appm He/dpa and triple ion beams of 15 or 150 appmHe/dpa and 50 or 1000 appmHe/dpa. These swelling were ranged from about 0.1% to 3%, and the swelling was enhanced by the synergistic effect of helium, hydrogen and displacement damage under the triple ion beams.

In present study, swelling behavior is examined at temperatures of 360 and 430°C to 50 dpa under dual ion beams. Figs. 3.6(a) and 3.6(b) show microstructures of F82H steels formed at 360 and 430°C to 50

dpa by dual ion beams of Fe and He ions, respectively. The microstructures formed by 360°C irradiation in F82H steel were only dislocation loops as shown in Fig. 3.5(a). Many cavities and dislocation loops were formed in F82H irradiated at 430°C to 50 dpa, and the swelling was about 0.6 %. The size distribution of cavies was bi-modal. In Fig. 3.7, the swelling of F82H irradiated by dual ion beams is given as a function of temperature, and the swelling peak temperature is around 430°C.

In previous studies of swelling by neutron irradiation [12,15], the effect of helium production on swelling of F82H irradiated at 300 and 400°C to 51 dpa by neutrons in HFIR (High Flux Isotope Reactor) was examined by using a ^{10}B doping technique. The swelling at 400°C tended to increase from 0.1 to 1.1 % with increasing helium production from about 10 to 330 appm, and the swelling at 300°C was very low and small cavities with low number density was formed in F82H steel with a helium production of about 330 appm. In the previous swelling study due to helium production in F82H steel, the ratio of helium production to displacement damage was not controlled during irradiation In this study, the ratio of helium to displacement damage was controlled during irradiation, and the relatively somewhat larger swelling was measured at around 430°C in the specimens irradiated by the dual ion beams.

3.3.3 Effect Helium on Fracture Behavior at High Temperature by SP Test

Figs. 3.8(a) and (b) show microstructures taken under low and high magnifications, respectively, by a transmission electron microscope for F82H steel implanted to about 84 appm helium and about 0.03 dpa by 50 MeV He^{2+} ions at about 120°C using an energy degrader of aluminum foils for helium ions. In the micrographs, dislocations, carbides, lath boundaries and small defect clusters like dislocation loops were observed. The number density of small defect clusters formed by the irradiation was very low. Cavities were not observed in the specimen.

The curves of load-displacement for the SP tests at 600 and 700°C in F82H steels after the helium implantation were given in Fig. 3.9. In the specimens implanted with helium, larger stress occurred as seen in Figs. 3.9(a) and 3.9(b), especially in the specimen tested at 600°C. In the helium-implanted specimens, the elongations were not degraded. After the SP tests, the fracture surfaces were observed by SEM as shown in Figs. 3.10 and 3.11. The ductile fracture surfaces were observed in all specimens. No cracking at grain boundaries were observed in all specimens tested at 600 and 700°C. Small cavities like blister at the cracked region were formed near outside the surface of the non-helium-implanted specimen tested at 700°C, however, such cavities were not observed in the helium-implanted specimen tested at 700°C. The formation of the cavities near the surface after SP test was also observed in only non-helium-implanted specimen tested at 600°C.

3.3.4 Effect of Helium Production on Fracture Toughness of F82H Steel

Fig. 3.12 shows ΔYS due to neutron irradiation in F82H+^{11}B, F82H+^{10}B+^{11}B and F82H+^{10}B steels irradiated at 300°C to 2.3 dpa as reported in previous study [3]. The tensile test temperatures were performed at 20, 300 and 400°C. Small increment of ΔYS due to helium production was observed in F82H+^{10}B steel with produced helium about 330 appm. Similar results are obtained in present study of ion irradiation experiment and the other studies as described in section 3.3.1. Therefore, helium production can be affect on microstrucutral evolution and irradiation hardening.

In this study, the effect of helium production on fracture toughness has been examined. Fig. 3.13 shows curves of load and displacement of fracture toughness specimens tested at 300°C in the F82H+^{11}B and F82H+^{10}B steels irradiated at 300°C to 2.3 dpa. The amounts of helium production in F82H+^{11}B and F82H+^{10}B steels are about 5 appm and 330 appm, respectively. The maximum loads of the irradiated F82H+^{11}B and F82H+^{10}B steels were about 2.5 and 2.9 kN, respectively, and the value of F82H+^{10}B steel was larger than it. As exceeded the maximum load, the strength of F82H+^{11}B steel was gradually decreased, while that of F82H+^{10}B steel was rapidly decreased and the fracture proceeded to the end of specimen after the displacement of only 2.2 mm. SEM micrographs after the fracture tests at 300°C are shown in Fig. 3.14. The surface of F82H+^{11}B steel with no helium production was relatively smooth, but the fracture surface of F82H+^{10}B steel with helium production was very rough. The cause would be related to the occurrence of sub- boundary crack due to helium migration to sub-boundaries. Brittle fracture surfaces of F82H+^{11}B and F82H+^{10}B steels were observed at –40°C and 100°C, respectively. The difference of temperature was about 140°C. The fracture surfaces of F82H+^{11}B and F82H+^{10}B steel in the brittle temperature regions were observed by a SEM as given in Fig. 3.15. The surface of F82H+^{11}B steel with no helium production was cleavage, but F82H+^{10}B steel with helium production was somewhat rough on the fracture surface.

3.3.5 Design Window of Martenisitic Steels for Irradiation Environment Systems

The result for the enhancement of hardening without degradation due to helium at high temperature is very important. In martensitic steel, the decrease of creep strength at higher temperature is one of negative properties. The design window of safety zone map for operation in fusion nuclear reactor using a water coolant system or other systems, based on data and knowledge about properties of reduced-activation ferritic/martensitic steels, was restricted at higher temperature by loss of creep strength or softening during irradiation [1]. However, the strength at higher temperature in the helium content specimen is larger than that in the non-content helium specimen, therefore, the safety zone at higher temperature may be modified by the suppression of deformation due to helium production.

The effects of helium production on swelling and fracture toughness as shown in sections of 3.2 and 3.4 can be also affected on the design window of martenisitic steels for irradiation environment systems, and the enhancement of swelling due to gas atoms and the shift of DBTT due to helium atoms are negative effects. We would have to take care of these effects to operate these systems as described in Fig. 3.16.

3.4 Summary

Effects of displacement damage and gas atoms on microstructures and mechanical properties of F82H steel were examined by some methods. The hardness of F82H was increased by triple beams, dual beams and single beam at 270°C to 20 dpa and 360°C to 50 dpa, and the increment of hardness by irradiation at 360°C was larger than that at 270°C. The increment of hardness due to triple, dual and single beams depended on the irradiation temperatures. The peak temperature of swelling induced by dual ion beams to 50 dpa was about 430°C at temperatures from 360 to 600°C and the value of swelling was about 0.6 %. Strength of F82H-std steel tested at 600 and 700°C by small punch (SP) was increased by about 84 appm helium implantation, and no degradation was observed. In fracture toughness test of 0.18DCT performed at 300°C of ductile properties, strengths of F82H with helium production was rapidly decreased as compared to that with no helium production beyond a maximum strength in ductile temperature region. The cause would be related to the occurrence of sub- boundary crack due to helium migration to sub-boundaries. From these results, the modification of safety zone of F82H steel for operation of nuclear environment systems is proposed.

3.5 References

1) M. Kawai, J. Nucl. Mater., 318(2003)371.
2) A. Hishinuma, A. Kohyama, R.L. Klueh, D.S. Gelles, W. Dietz and K. Ehrlich. *J. Nucl. Mater.* **258–263** (1998)193.
3) E. Wakai, S. Jitsukawa, H. Tomita, K. Furuya, M. Sato, K. Oka, T. Tanaka, F. Takada, T. Yamamoto, Y. Kato, Y. Tayama, K. Shiba, S. Ohnuki, J. Nucl. Mater.,in press.
4) M. Rieth, B. Dafferner and H.D. Rouhrig. *J. Nucl. Mater.* **258–263** (1998)1147.
5) D.S. Gelles. *J. Nucl. Mater.* **283–287** (2000)838.
6) E.I. Materna-Morris, M. Rieth, K. Ehrich, Effects of Radiation on Materials, STP1366, p. 597
7) K. Shiba, I. Ioka, J.P. Robertson, M. Suzuki, A. Hishinuma, Euromat-96, (1996)265.
8) E. Wakai, K. Kikuchi, S. Yamamoto, T. Aruga, M. Ando, H. Tanigawa, T. Taguchi, T. Sawai, K. Oka, S. Ohnuki, J. Nucl. Mater., 318(2003)267.
9) E. Wakai, T. Sawai, K. Furuya, A. Naito, T. Aruga, K. Kikuchi, S. Yamashita, S. Ohnuki, S. Yamamoto, H. Naramoto and S. Jitsukawa. *J. Nucl. Mater.* **307–311** (2002)278.
10) T. Sawai, E. Wakai, K. Tomita, A. Naito and S. Jitsukawa. *J. Nucl. Mater.* **307–311** (2002)312.
11) T. Tanaka, K. Oka, S. Ohnuki, S. Yamashita, T. Suda, S. Watanabe, E. Wakai, J. Nucl. Mater., 329-333(2004)294.
12) E. Wakai, N. Hashimoto, Y. Miwa, J.P. Robertson, R.L. Klueh, K. Shiba and S. Jitsukawa. *J. Nucl. Mater.* **283–287** (2000)799.
13) Y. Miwa, E. Wakai, K. Shiba, N. Hashimoto, J.P. Robertson, A.F. Rowcliffe and A. Hishinuma. *J. Nucl. Mater.* **283–287** (2000), p. 334.
14) T. Morimura, A. Kimura, H. Matsui, J. Nucl. Mater., 239(1996)118-125.
15) E. Wakai, Y. Miwa, N. Hashimoto, J.P. Robertson, R.L. Klueh, K. Shiba, K. Abiko, S. Furuno and S. Jitsukawa, J. Nucl. Mater., 307-311(2002)203.
16) M. Ando, E. Wakai, H. Tanigawa, T. Sawai, K. Furuya, S. Jitsukawa, H. Takeuchi, K. Oka, S. Ohnuki, A. Koyama, J. Nucl. Mater.,329-333(2004)1137.
17) Y. Katoh, H. Taniga wa, T. Muroga, T. Iwai and A. Kohyama. *J. Nucl. Mater.* **271–272** (1999), p. 115.
18) M. Ando, H. Tanigawa, S. Jitsukawa, T. Sawai, Y. Katoh, A. Kohyama, K. Nakamura and H. Takeuchi. *J. Nucl. Mater.* **307–311** (2002), p. 260.
19) J. Henry, X. Averty, Y. Dai, P. Lamagnere, J.P. Pizzanelli, J.J. Espinas, P. Wident, J. Nucl. Mater., 318(2003)215.
20) N. Hashimoto, J.D. Hunn, T.S. Byun, L.K. Mansur, J. Nucl. Mater., 318(2003)300.
21) K. Farrel, T.S. Byun, J. Nucl. Mater., 318(2003)274.
22) E. Wakai, T. Taguchi, T. Yamamoto, H. Tomita, F. Takada, S. Jitsukawa, Materials Transactions, JIM, 46(2005)481.
23) E. Wakai, S. Matsukawa, T. Yamamoto, Y. Kato, F. Takada, M. Sugimoto, S. Jitsukawa, Materials Transactions, 45-8(2004)2641.

24) Y. Dai, X.J. Jia, K. Farrel, J. Nucl. Mater., 318(2003)192.

25) S.A. Maloy, M.R. James, W.R. Johnson, T.S. Byun, K. Farrel, M.B. Toloczko, J. Nucl. Mater., 318(2003)283.

26) R. Kasada, A. Kimura, H. Matsui and M. Narui. *J. Nucl. Mater.* **258–263** (1998), p. 1199.

27) R.L. Klueh, M.A. Sokolov, K. Shiba, Y. Miwa and J.P. Rpbertson. *J. Nucl. Mater.* **283–287** (2000), p. 478.

28) T. Sawai, M. Ando, E. Wakai, K. Shiba, S. Jitsukawa, Fusion Science and Technology 44-1(2003)201.

29) A. Kimura, T. Morimura, R. Kasada, H. Matsui, A. Hasegawa, K. Abe, "Effects of Radiation on Materials", 19th symposium, p.626.

30) N.Yamamoto, J. Nagakawa and K. Shiba, J. Nucl. Mater., 283-287(2000)400.

31) N.Yamamoto, Y. Murase, J. Nagakawa and K. Shiba, J. Nucl. Mater., 307-311(2002)217.

32) W.D. Oliver and G.M. Pharr. *J. Mater. Res.* **7** (1992), p. 1564.

33) Y. Miwa, et al., JAERI-Review 97-015(1997)108.

34) E. Wakai, T. Taguchi, T. Yamamoto and F. Takada, J. Nucl. Mater., 329-333(2004)1133-1136.

35) E. Wakai, T. Taguchi, T. Yamamoto, Y. Kato, F. Takada, Materials Transactions 45-8(2004)2638.

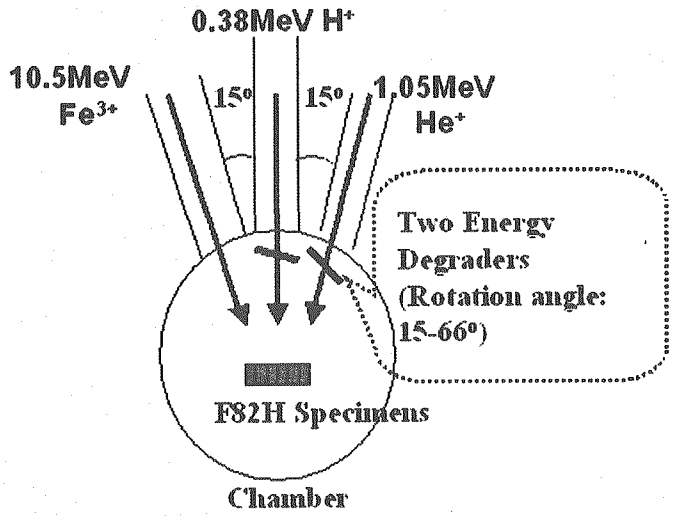

Fig. 3.1 Schematic configuration of three beam lines, two energy degraders and specimens. The ratios of He/dpa and H/dpa were controlled by degraders.

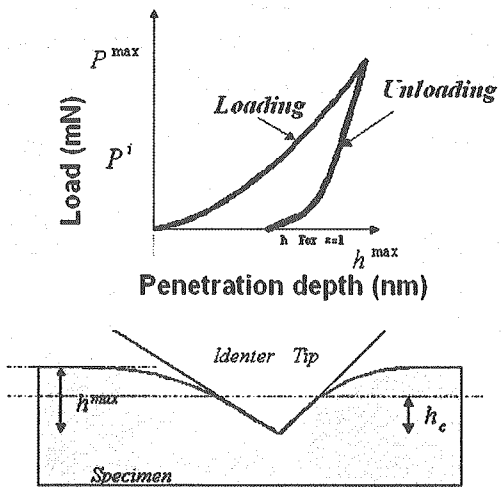

Fig. 3.2 The direction of indentation was chosen to be parallel to the ion beam axis or normal to the irradiated surface. The shape of the indenter tip was a Berkovich tip.

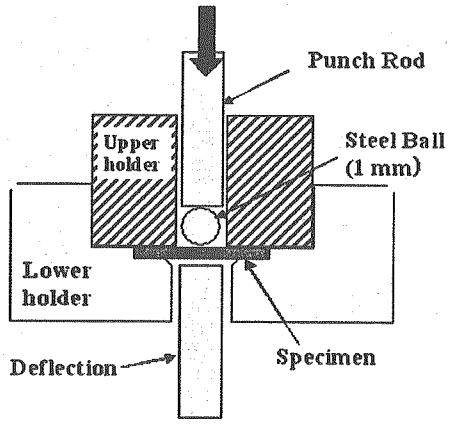

Fig. 3.3 Small punch testing machine and ϕ 3 mm specimen.

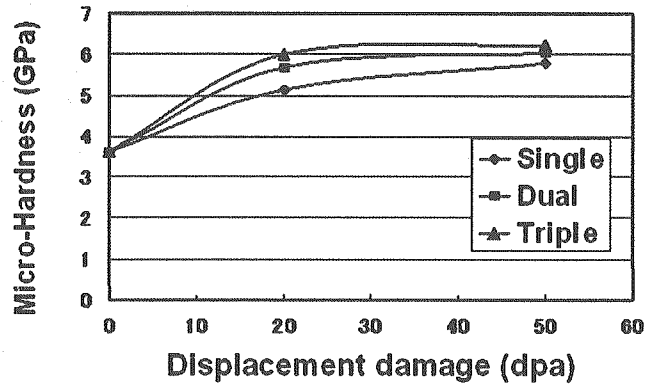

Fig. 3.4 Changes of hardness of F82H steel irradiated at 360°C to 50 dpa under single, dual and triple beams in TIARA facility.

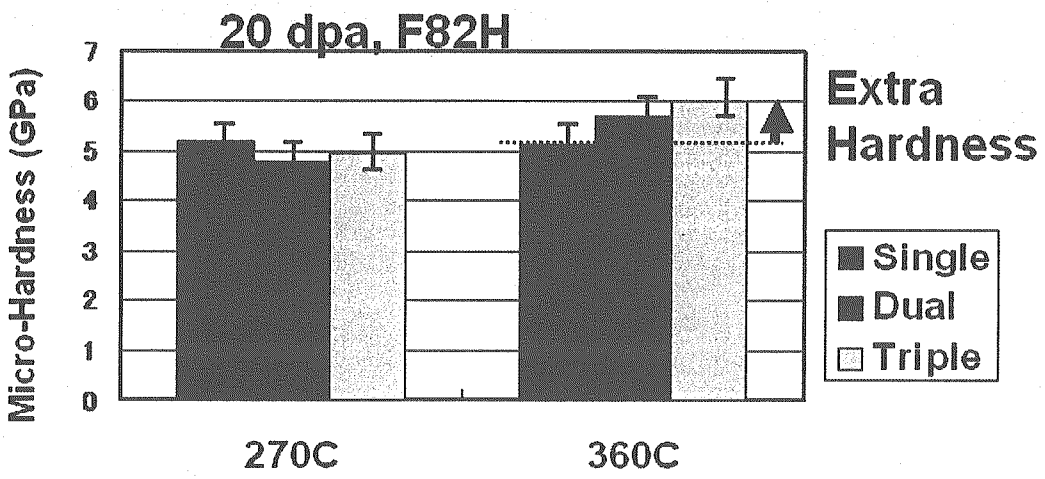

Fig. 3.5 Changes of hardness of F82H steel irradiated at 270 and 360°C to 50 dpa.

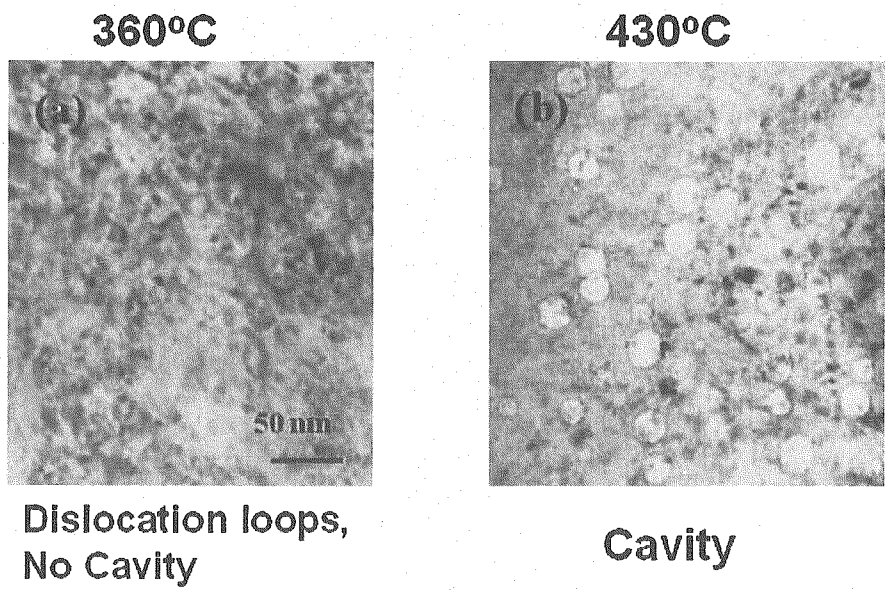

Fig. 3.6 Microstructures formed in F82H steels irradiated with dual beams at (a) 360°C and (b) 430°C to 50 dpa

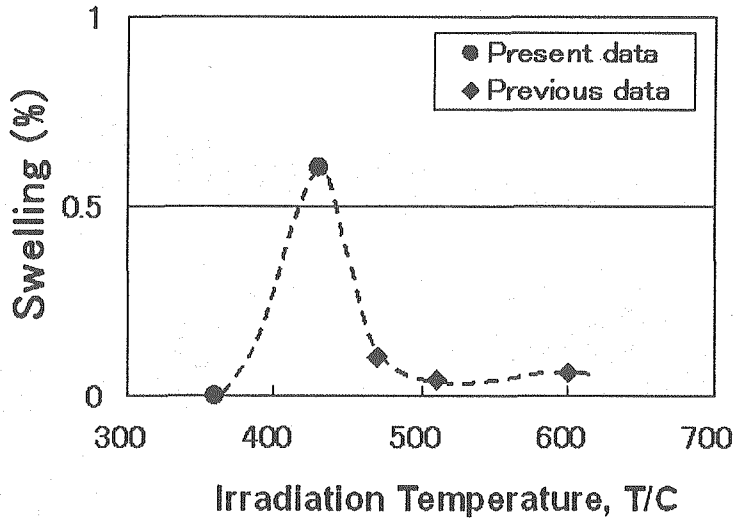

Fig. 3.7 Dependence of irradiation temperature for swelling of F82H steel irradiated with dual beams to 50 dpa.

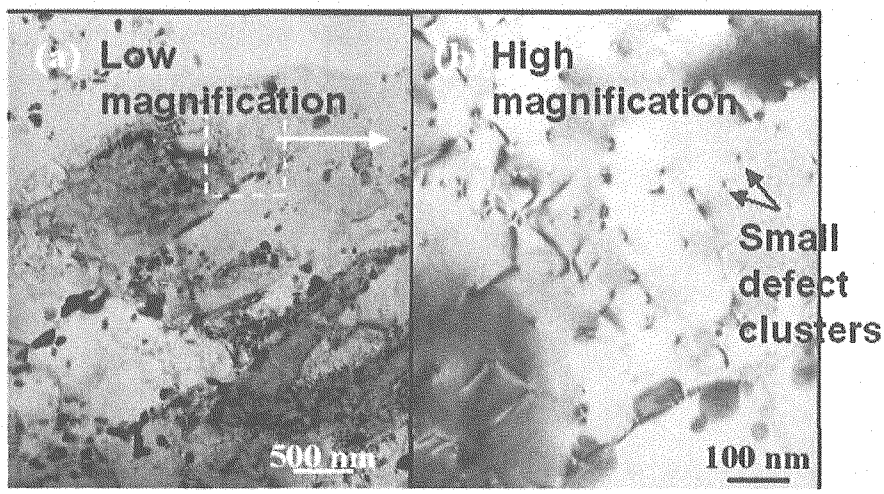

Fig. 3.8 Microstructures of (a) low and (b) high magnification figures in F82H steel implanted with 50 MeV He^{2+} ions at 120°C to 0.03 dpa.

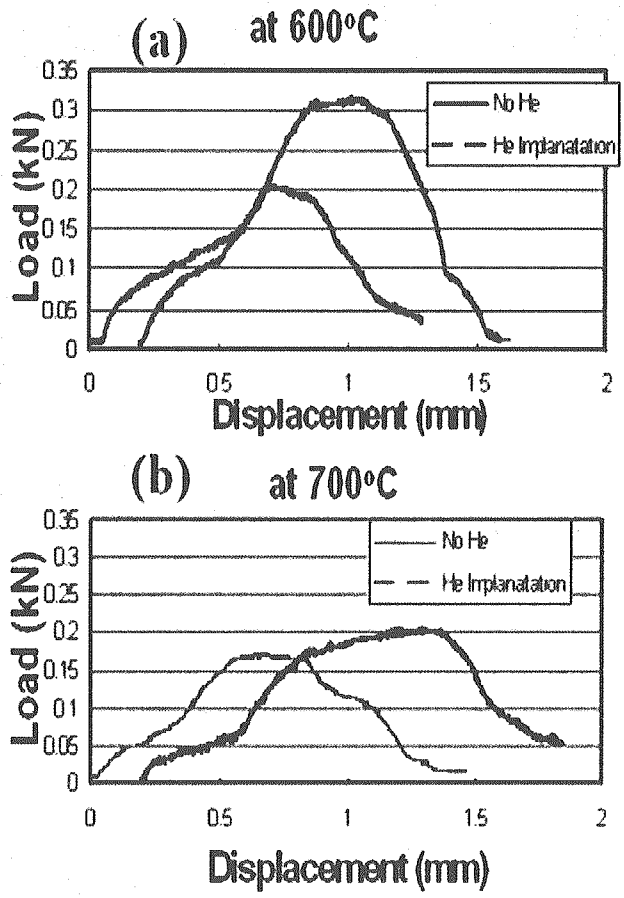

Fig. 3.9 Curves of load-displacement for the SP tests at 600 and 700°C in F82H steels after the helium implantation.

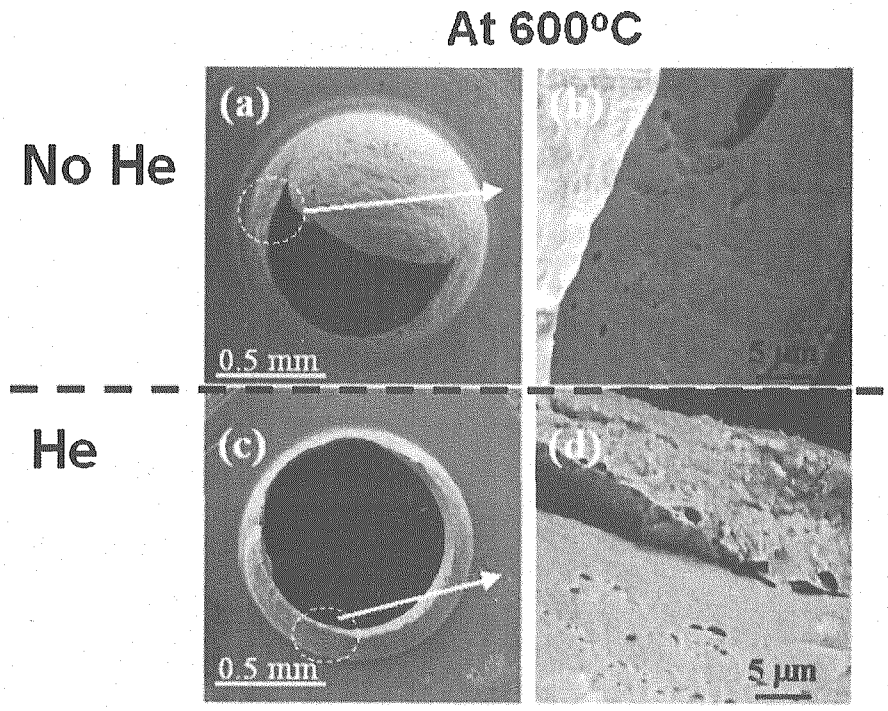

Fig. 3.10 SEM micrographs of (a) no-helium and (b) helium implanted F82H specimens tested at 600°C after small punch.

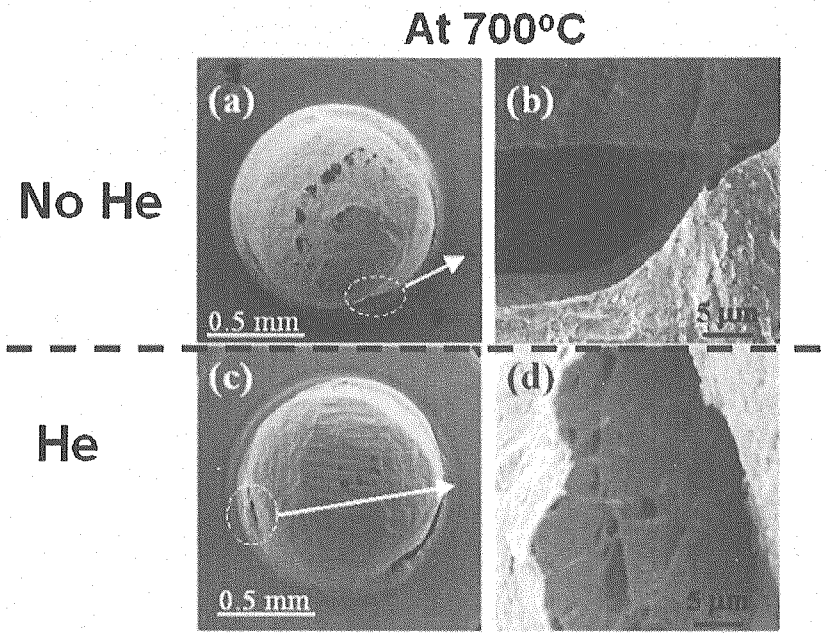

Fig. 3.11 SEM micrographs of (a) no-helium and (b) helium implanted F82H specimens tested at 700°C after small punch.

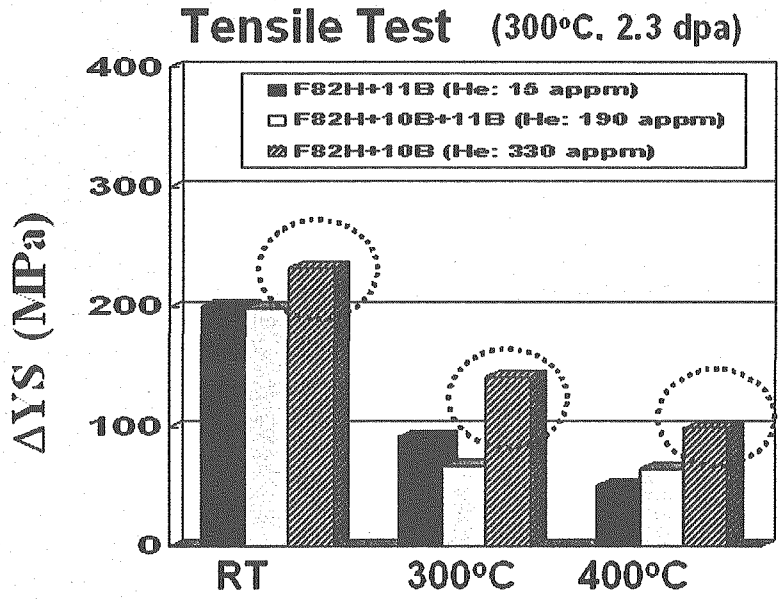

Fig. 3.12 ΔYS due to neutron irradiation in F82H+^{11}B, F82H+^{10}B+^{11}B and F82H+^{10}B steels irradiated at 300°C to 2.3 dpa.

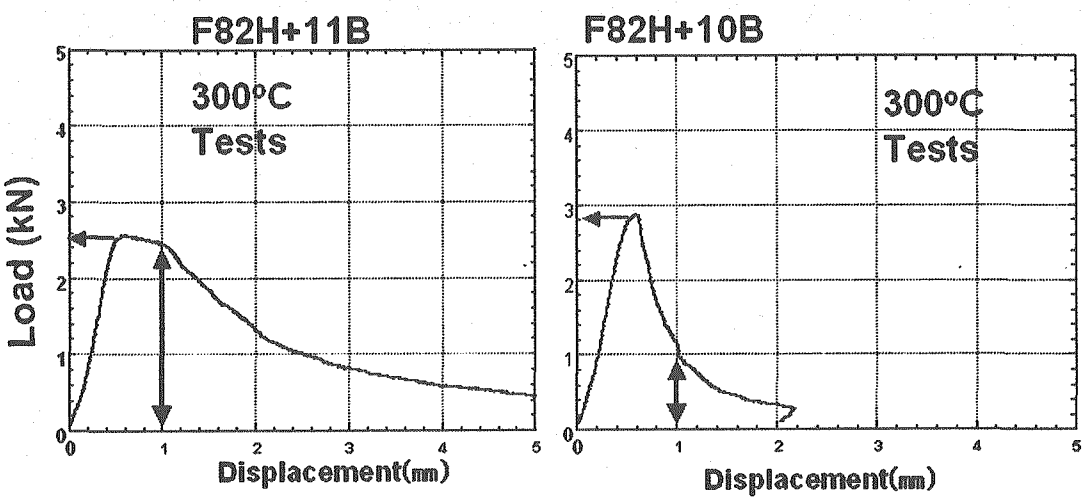

Fig. 3.13 Curves of load and displacement of 0.18DCT fracture toughness specimens tested at 300°C in the F82H+^{11}B and F82H+^{10}B steels irradiated at 300°C to 2.3 dpa

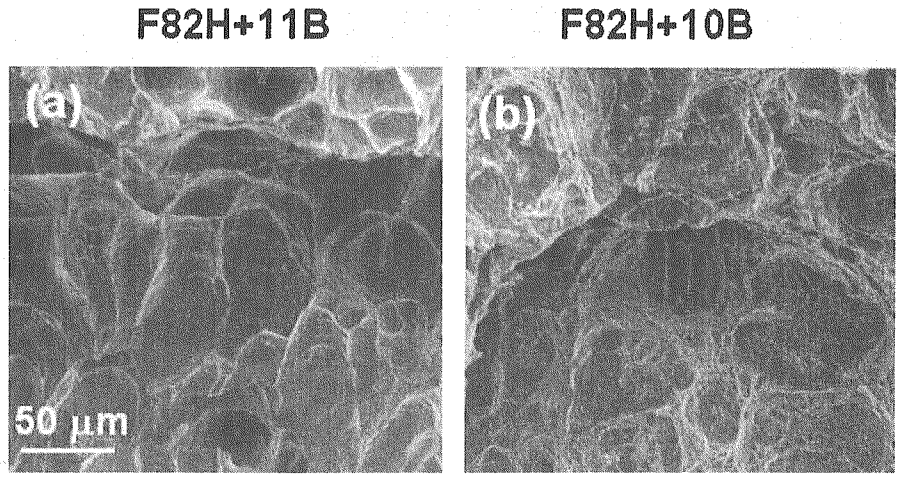

Fig. 3.14 SEM micrographs of F82H+^{11}B and F82H+^{10}B steels irradiated at 300°C to 2.3 dpa after the fracture testing at 300°C.

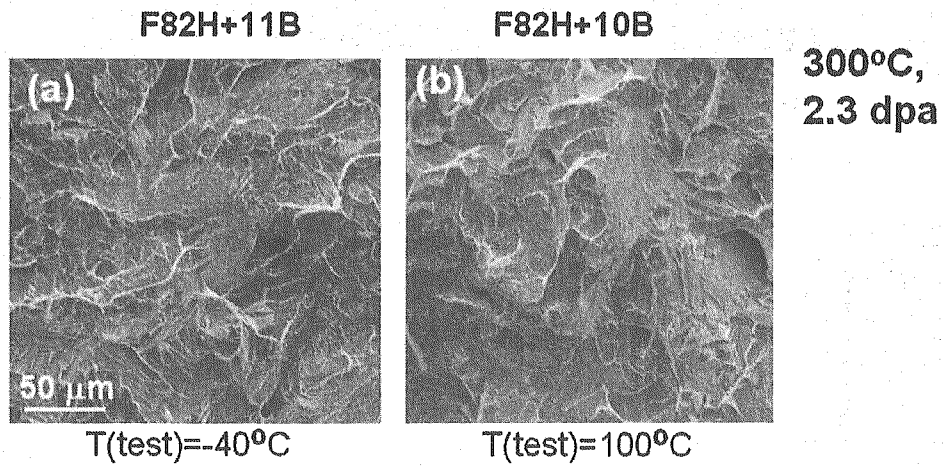

Fig. 3.15 SEM micrographs of F82H+^{11}B and F82H+^{10}B steels irradiated at 300°C to 2.3 dpa after the fracture testing at lower temperature.

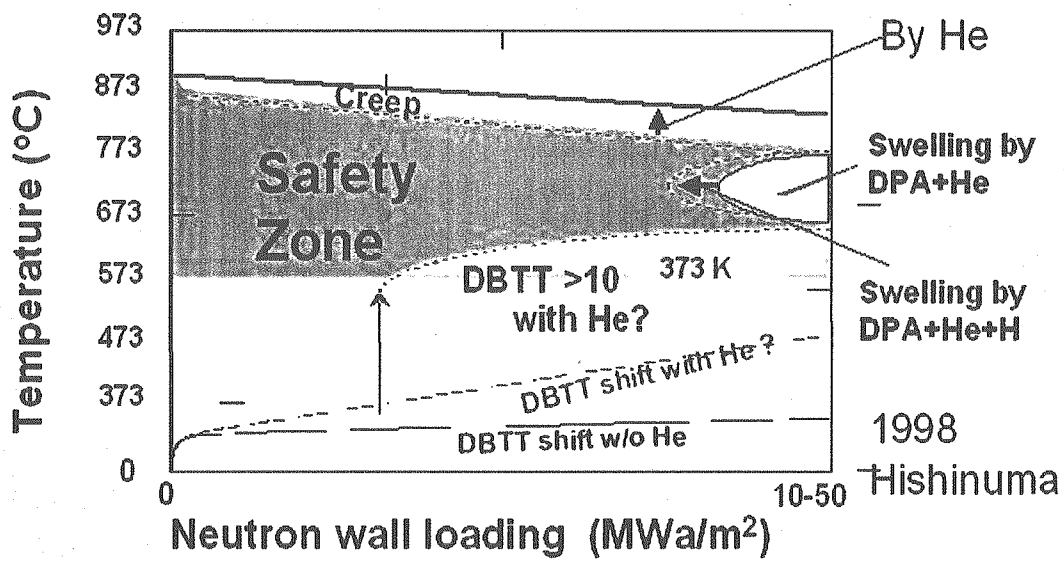

Fig. 3.16 Modification of design window of martenisitic steels for irradiation environment systems.

Table 3.1: Chemical compositions of F82H-std and F82H doped with ^{10}B, ^{11}B and $^{10}B+^{11}B$ steels used in this study (wt%)

Materials	B	C	Si	Mn	P	S	Cr	W	V	Ta
F82H	0.0002	0.09	0.07	0.1	0.003	0.001	7.82	1.98	0.19	0.04
F82H+^{10}B	0.0061	0.097	0.10	0.10	0.007	0.001	7.96	1.98	0.18	0.05
F82H+^{11}B	0.0059	0.093	0.11	0.10	0.007	0.001	8.02	1.98	0.18	0.05
F82H+$^{10}B+^{11}B$	0.0067	0.094	0.12	0.90	0.007	0.001	8.01	2.01	0.18	0.05

4. Information of Neutron Irradiation of 04M-67A and 04M-68A capsules in JMTR

Capsules of 04M-67A and 04M-68A were manufactured in JAERI in 2004. Neutron irradiation was performed from 157 cycle to 160 cycle in 2005, and the total time of irradiation was about 2,766 hours. The irradiation temperatures of the 04M-67A and 04M-68A were approximately 250°C and 350°C, respectively. The positions of the capsules of 04M-67A and 04M-68A in the JMTR were K-10-2 and K-10-3, respectively. The estimated fast and thermal neutrons at a peak value in the capsule of 04M-67A were 1.23×10^{25} m^{-2} and 2.87×10^{25} m^{-2}, respectively. The estimated fast and thermal neutrons at a peak value in the capsule of 04M-68A were 1.23×10^{25} m^{-2} and 2.97×10^{25} m^{-2}, respectively. F82H-std steel, F82H+60ppm ^{10}B steel and F82H+60ppm ^{11}B steel were used in this experiments, and tensile specimen of SS-3 type, Charpy impact specimens of 1/3CVN and t/2-1/3CVN, fracture toughness specimens with pre-crack of t/2-1/3PCCVN, DFMB and 0.18DCT and TEM specimens for SP test and microstructural observations were irradiated in the capsules.

Acknowledgements

The author is grateful to Messes. F. Takada, Y. Kato, T. Yamamoto, H. Tomita and the other members of JMTR hot laboratory of JAEA for assistance with the experimental works. Many productive discussions with Drs. T. Sawai, H. Tanigawa and N. Okubo are also gratefully acknowledged.

Appendix I (New Machine for Small Fracture Toughness Specimens)

A new test machine of small fracture toughness specimens of 1/3PCCVN and DFMB types has been manufactured to examine the fracture toughness and DBTT (ductile-brittle transition temperature) of small size specimens of reduced-activation ferritic/martenisitc steels. This machine can be operated at temperatures from −180°C to 300°C in air. The accuracy of the control for the specimen position is basically less than one micron. The maximum value of load is 2 kN. The performance of the machine for the measurement of displacement of specimen position and cross head position, the control of temperature and etc was checked by using some specimens of 1/3PCCVN and DFMB, and it was modified through our tests. The design of the machine manufacture of the fracture toughness tests for the irradiated specimens was reflected through this modification process. The detail of this procedure was described in Japanese as following contents.

A.1 試料変位の測定

本装置での試料の変位測定には、光学的手法を用いた。ここで用いた方法は、ＬＥＤから発生した平行光をＣＣＤで受け、その間にセットした試料の動きから変位を求めている（キーエンス社 LS-7000 シリーズ使用）。

この検出器は、高精度（±0.15μm）、高速サンプリング（2400 回／秒）という基本性能を有する。この方法は試料を直接、試料の動きを捉えるという利点を有する。試料は通常、低温に保持されるために恒温槽中の試料ステージにセットしているが、透明なガラス窓を通して、恒温層の外側から試料を観察できるようにしてある。なお、測定器は恒温槽の外側に設置し、光路上に恒温槽のガラス窓が設けられている。また、変位測定のポイントは、試料中心のノッチ部から少し右（または左）に少しずらした位置でセットする方法を取った。き裂の開口部が、変形中に、変位測定の妨げになるからである。開口変位やＺ軸方向の変位は、クロスヘットに取付けた変位計(Mitsutoyo 製)と光学変位計（キーエンス製）の双方から評価する必要がある。

なお、本装置の性能確認用の測定試料には、核融合炉構造材料として開発しているＦ８２Ｈ鋼(Fe-8Cr-2W-0.1C 系マルテンサイト鋼)を用いた。また、試験片の種類としては、微小な DFMB(L=20mm)及び t/2-1/3PCCVN(L=20mm)の２種類の試験片を用い、装置の性能及びこれらの試験片の靭性を合わせて評価した。

A. 2 Noise of Measurement of Displacement occurred at the initial set 設置初期に現れた変位ノイズ

本微小試験装置は、設置当初に、測定された変位ノイズの典型例を図Ａ．１に示す。試料はＦ８２Ｈ鋼を用い、約－１５０℃で３点曲げを除荷コンプライアンス法によって試料の荷重と変位を制御した。この時に、荷重－変位曲線の一部である除荷の過程に対して、時間スケールを短くして、変位と荷重の様子を調べたものであるが、大きなノイズを有して、制御がうまくいっていないことが分かった。この変位の時間変化を調べたものを図Ａ．２に示した（横軸は時間スケール）。１０μｍを越えるスパイク状の異常な変位が現れていることが分かった。このスパイク的な変位は、周期的な要素が有るように思われたので、振動解析した。その結果を図Ａ．３に示す。周期２秒および１秒の処に顕著な振動が存在していた。この主な原因は、低温で動作する冷却用の液体窒素（ガス）を供給する電磁弁による振動であることが分かった。このため、電磁弁を干渉材で包む対応を取った。さらに、振動を除去するためは、電磁弁と本体を結ぶ配管をフレキシブルチューブに代え、電磁弁の固定方法を変えて、振動が伝わりにくいような対応が必要である。この点は、すでにホットセル用の装置設計に取り入れた。

他方、この変位ノイズを信号処理によって低減する試みを行った。一つはロードセルの動作をフィードバックさせてコントロールする方法である。フィードバックの強さを弱めると、変位ノイズは低減した。このことから、ノイズに対する変位制御のフィードバックが過剰に反応していた可能性があることが分かった。さらに、変位制御の回路に、フィルター作用を取り入れることによって、そのような振動は、図 A. ４に見られるように、かなり低減できることも分かった。

しかしながら、図A．４における信号は、合理的な変位制御を行った場合の変位曲線から外れていると考えられる。この問題は次節で論ずる。

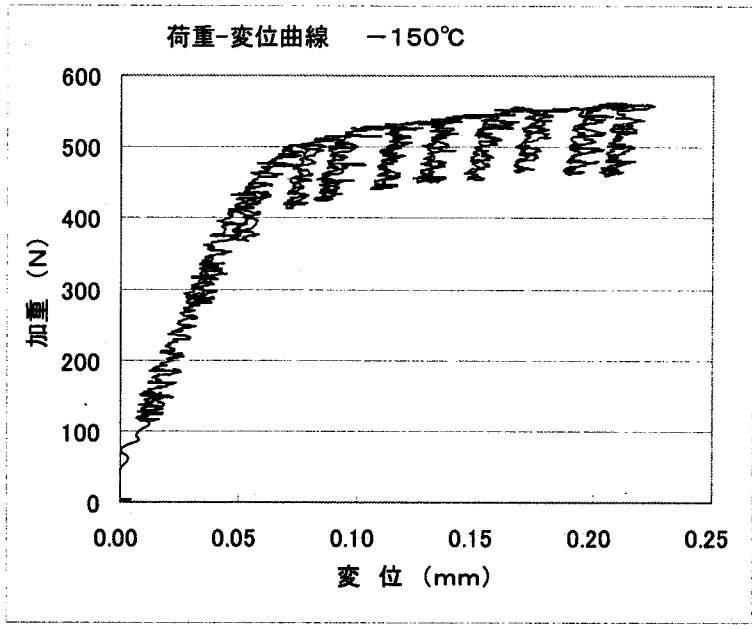

Fig. A.1　Signals of load-displacement curve at the first stage of the machine manufacture.

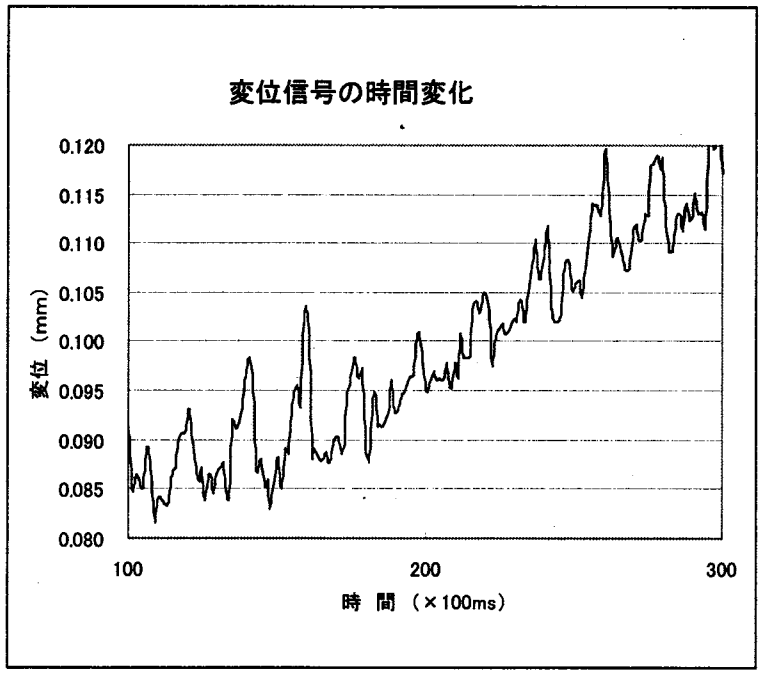

Fig. A.2　Signal of displacement to time in a short period.

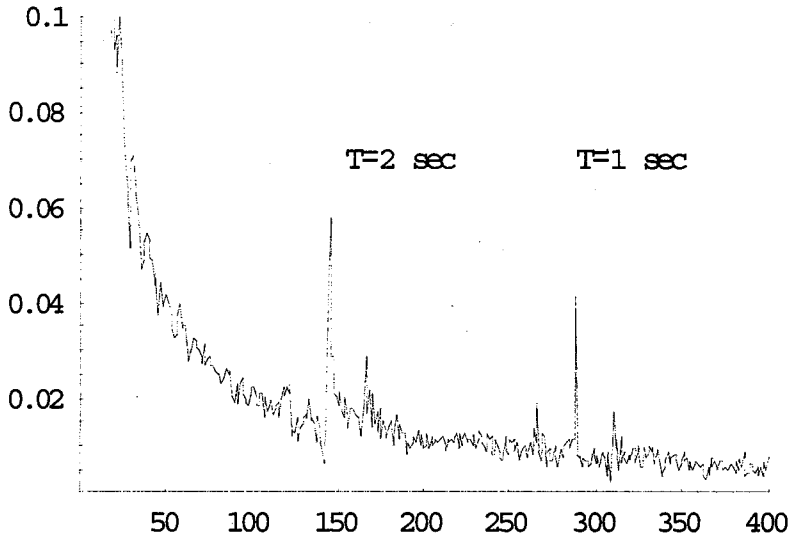

Fig. A.3 Oscillation spectrum of the signal of displacement to time at −150°C in a very short time. The values of the axes are arbitrary units. The periodical peaks was seen.

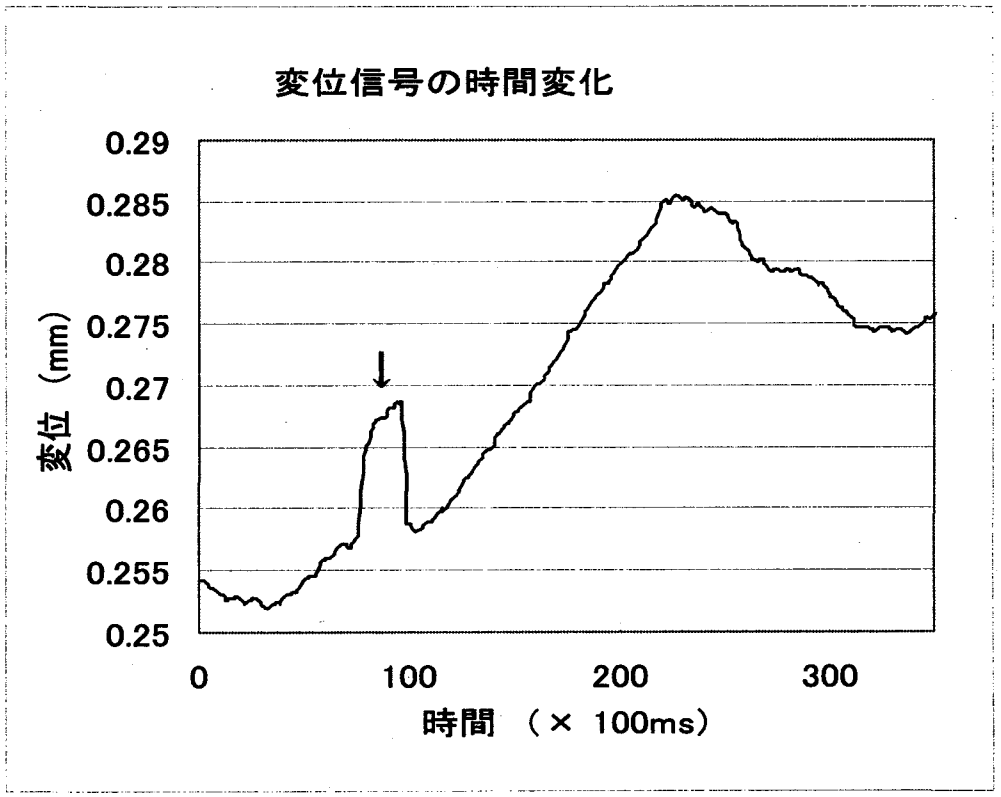

Fig. A.4 Improved curve of displacement to time at −150°C after the treatment of reduction of noise. The abnormal displacement remained as indicated by an arrow.

A. 3　光学的測定と冷却

ＲＴから－180℃の間で変位制御の精度を調べた。液体窒素温度に近づくにつれて、光で測定する試料の変位（光学的（ＬＥＤ）測定法）が時々、一瞬、大きく変動することが分かった。図Ａ.４には、不規則な信号が乗っているのが分かる（図中の矢印)。これは、冷却用の液体窒素の‘しぶき’状の塊がＬＥＤの光路を遮った事によるものであることが分かった。また、－１８０℃では非常に、頻繁に試料の変位が、一時的に大きくずれるが観測された。その結果を図 A. ５に示す。変位信号がスケールオーバーしている箇所は、液体窒素のしぶきの塊が光路に入って、光の信号が遮断されたためであった。本装置の温度コントローラは、－１５０℃以下の設定にすると、液体窒素の噴出孔から、ガスのみならず、液体の塊も出て行く割合が高くなっていくことが、詳しい観察から判明した。さらに、冷却時には、ガラス窓が曇らないように、いくつかの工夫が必要であり、試験前に水分が付着しないように窓枠を暖めた後、恒温槽内の温度を下げる手順を踏むことが大事である。

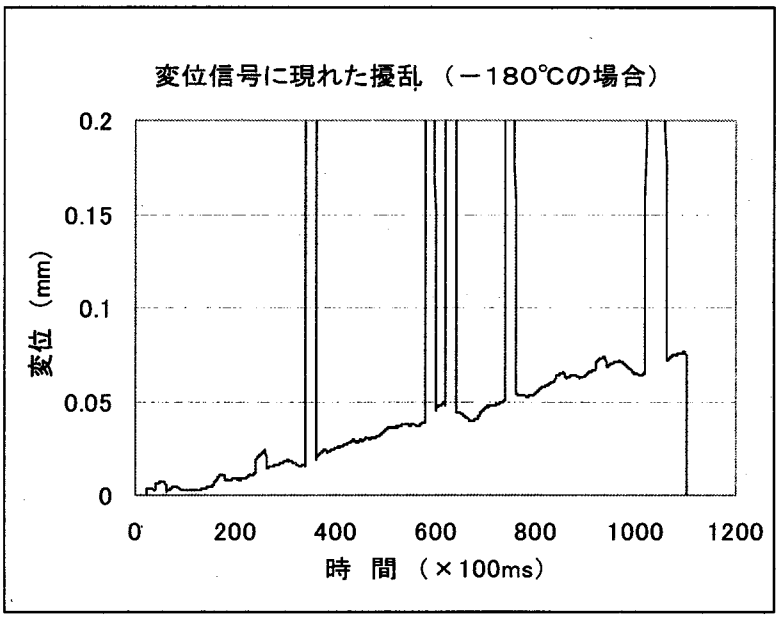

Fig. A.5　Signal of displacement to time measured at -180°C under the condition controlled by the optical system. The signal was sometimes lost.

A. 4　リニアゲージの評価

上記光学的測定に低温測定に対して限界があると考えられるため、他の方式の変位測定であるリニアゲージによる測定法を評価した。変位測定については、できるだけ試料の近く（槽内）に計測器を設けて、変位量を測定するべきであるが、大きな改造になるため、今回は槽の外にリニアゲージ（Mitutoyo LGF-525L）を設置して変位量を計測することにした。ただし、リニアゲージの信号出力が小さいことから、ノイズ問題が同様に発生したが、同様な対処法により、ノイズ低減を行った。

次に、このリニアゲージの変位を制御に使って、荷重－変位曲線を調べた結果を図A．６に示す。この場合の温度は－１８０℃であるが、前述の光学的変位制御の場合よりも、より適正に変位が制御できている様子を見ることができた。なお、荷重変位曲線を詳しく調べると、理想の制御からずれている様であり、まだ改善が必要と判断される。

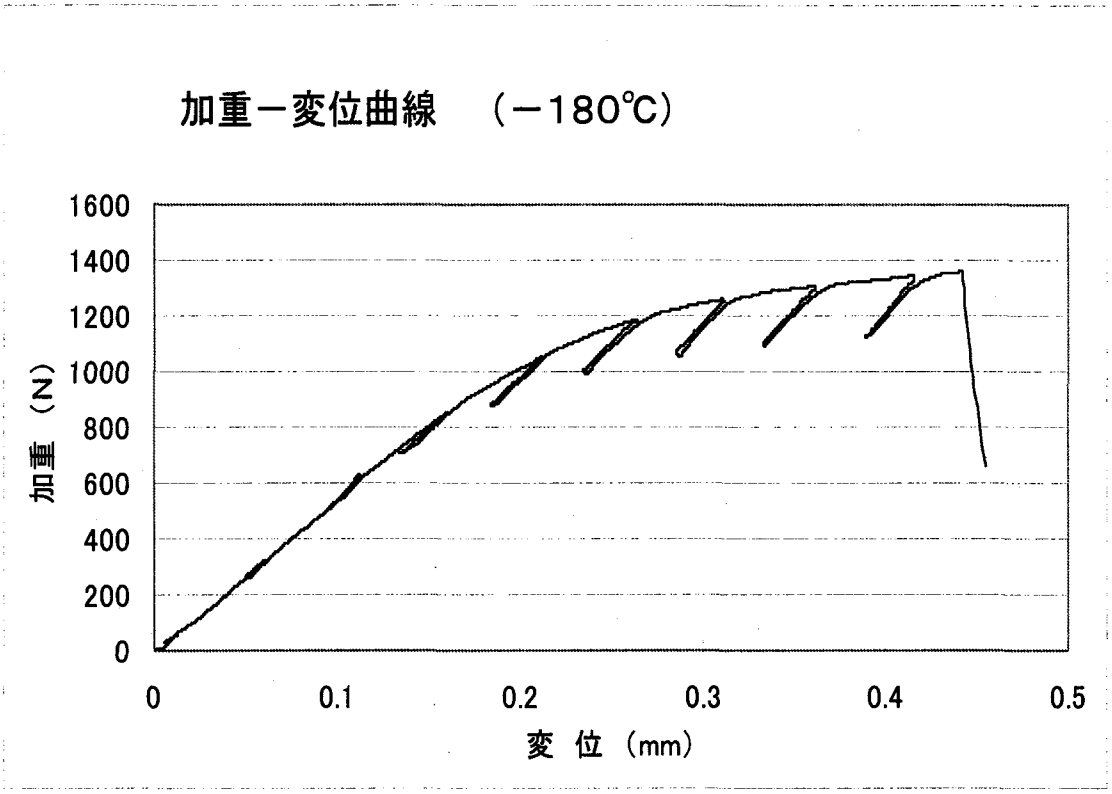

Fig. A.6　Curve of load-displacement at -180°C under the condition controlled by a linear gauge.

図 A. 7は加重－変位曲線を取った測定での、ＬＥＤ測定とリニアゲージの変位の関係を見たものである(時間的に進行)。荷重が一定方向に進んでいるときには、両者の関係は直線的である。しかし、除荷の時にはこの関係が破れて、ＬＥＤの変位に対してリニアゲージ上の変位は少なくなる。リニアゲージが測定する変位が減少しているので、変位がどこかで吸収されている可能性を示していると考えられる。おそらく、恒温槽内のクロスヘッド部と外部との温度差によって、リニアゲージが取り付けられているロードセルの腕などに発生している'たわみ'などによるものであろうと推測される。

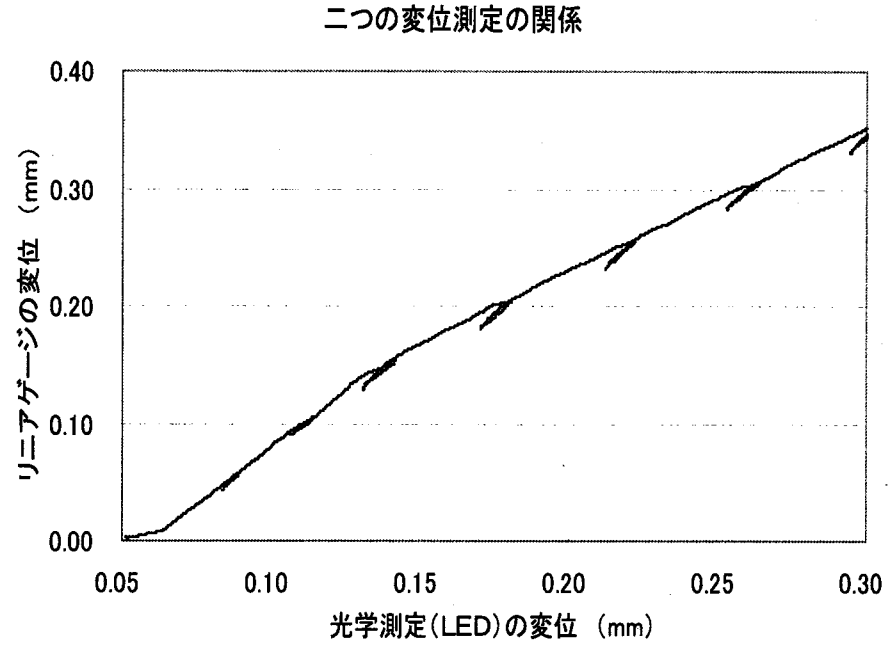

Fig. A.7 Relation between LED displacement and linear gauge displacement. There is a difference at the process of unloading.

図A. 8は、2つの変位計（光変位計(キーエンス製)とリニアゲージ(Mitsutoyo製)）によって測定した変位に対する荷重－変位曲線を比較したものである。除荷の時の傾きにおいて、二者の間に差が生じている。リニアゲージでは、たわみの影響が現れていると判断できるので、リニアゲージの変位制御のデータは、そのままでは解析に使えないことが判明した。

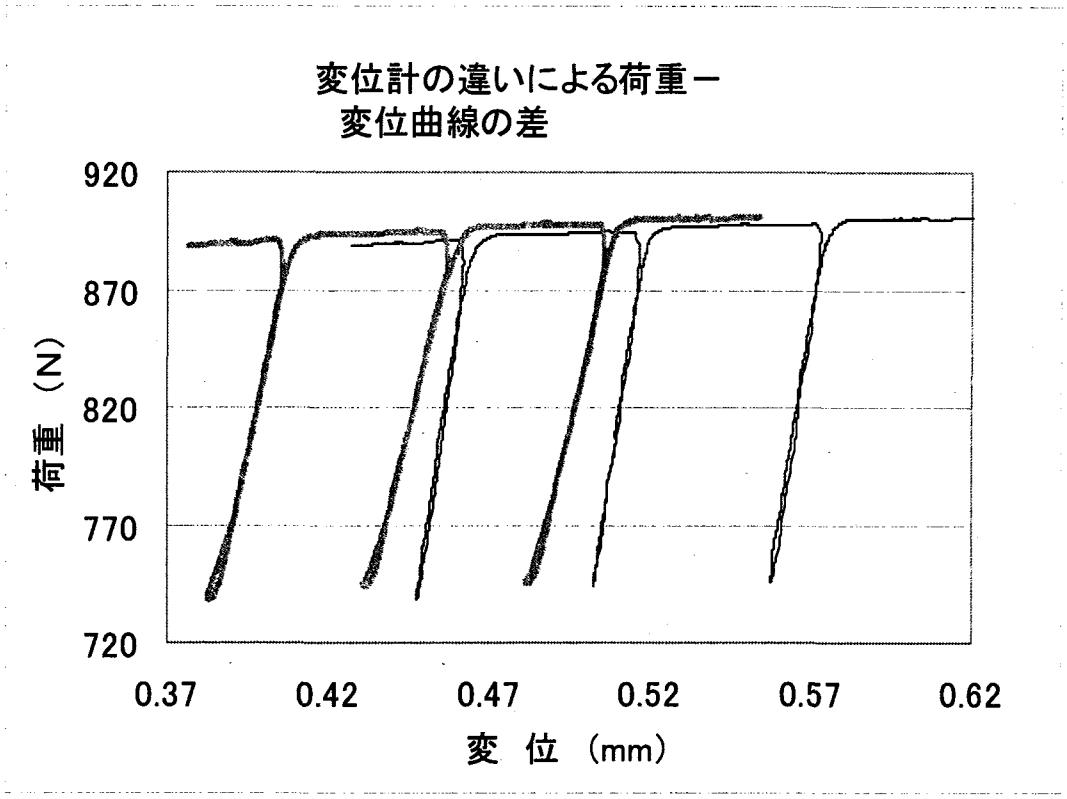

Fig. A.8 Comparison of load-displacement curves between the LED system and the linear gauge system. The slopes of unloading process for these systems were different. (The bold solid line is for the linear gauge system and the solid line is for the LED system.)

A. 5　ＬＥＤ信号の変位量の変換

この章の冒頭で述べたように、ＬＥＤが与える変位は試料中央のものではないので、スパン中央変位に変換する必要がある。ここでは二つの方法を試みる。一つは実測、もう一つは計算である。

実測にはリニアゲージを利用した。それが中央の変位を与えるからである。前節では、リニアゲージに低い評価を与えたが、これは除荷過程にある問題が生じていることを意味する。ただし、一方向に押すだけの場合で、たわみが'飽和'した後であれば、リニアゲージはその本来の性能を発揮しているとして良い。従って、たわみが飽和するまでを別の方法で決め、それを考慮すれな、中央変位はリニアゲージから求めることが出来る。この時のＬＥＤ信号を同時に得て、対応関係を得れば、その後のＬＥＤ信号は中央変位に変換されて得ることが出来る。

図 A. ９はそのようにして求めた中央変位の変換図である。この図には同時に、測定値を２次式でフィッティングした結果も重ね合わせてある。一本の線に見えて、良い一致を示している。次に、図A. １０に、LED 変位から中央変位を計算するときのモデルを示した。このようなモデルから、ＬＥＤ変位と中央部での変位の対応関係を計算した結果、２次式フィッティングに比してややずれがあり、もう少しモデルの検討が必要であることが分かった（図A. １１）。

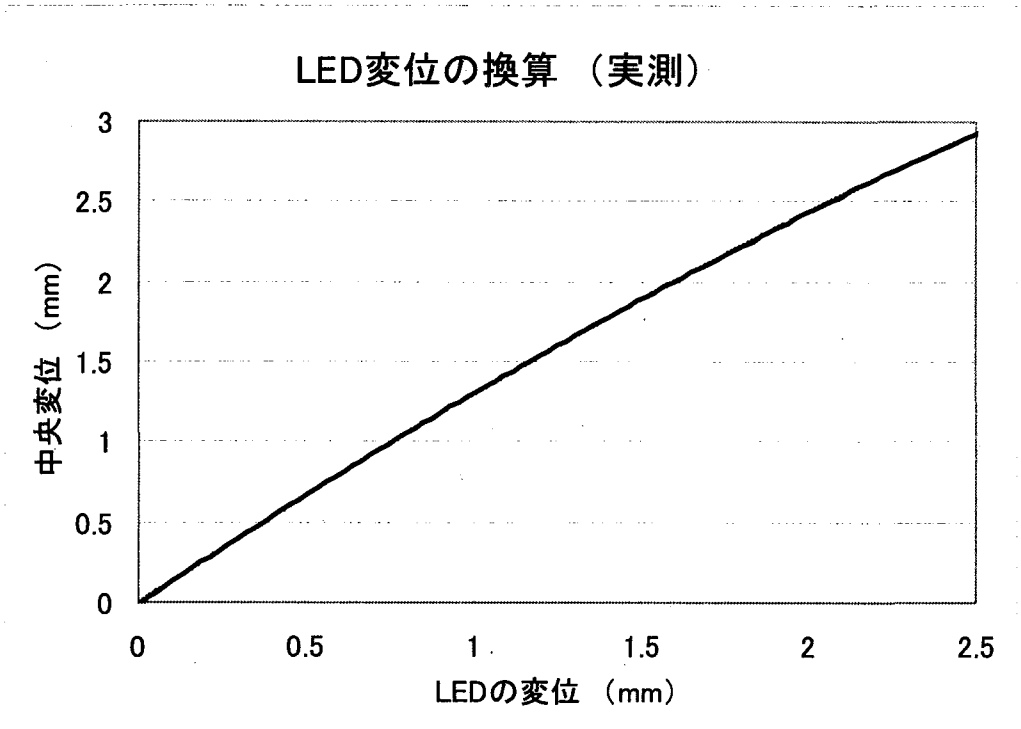

Fig. A.9　Relation between the position change of the measured LED system and the position change of the center of specimen.

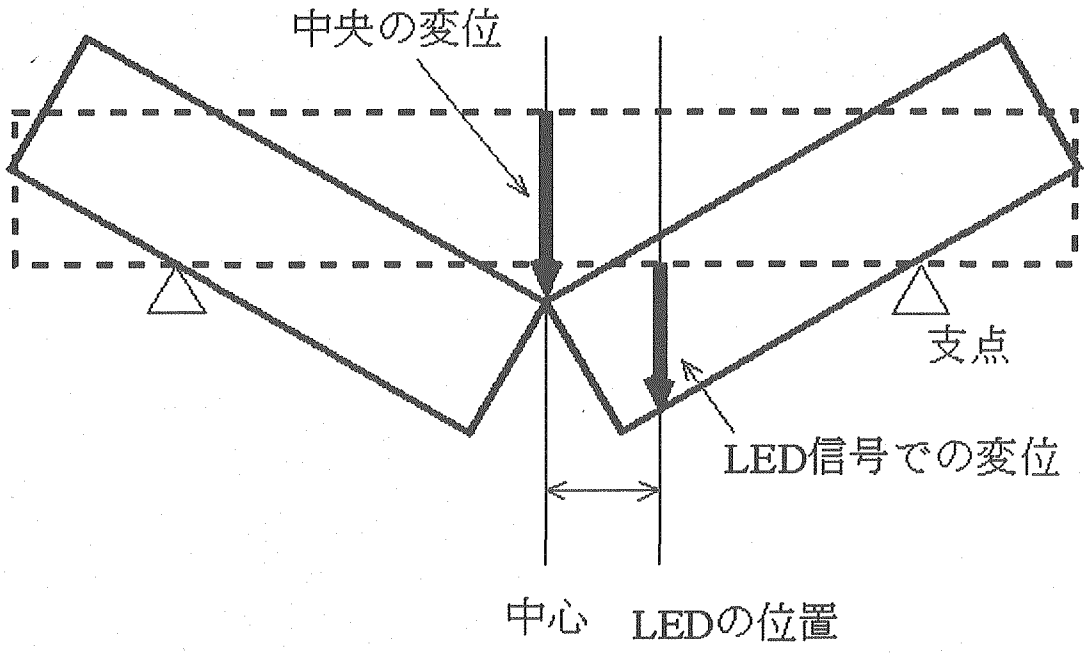

Fig. A.10 Calculation model for the conversion from the position measured by LED system to the position in the specimen center.

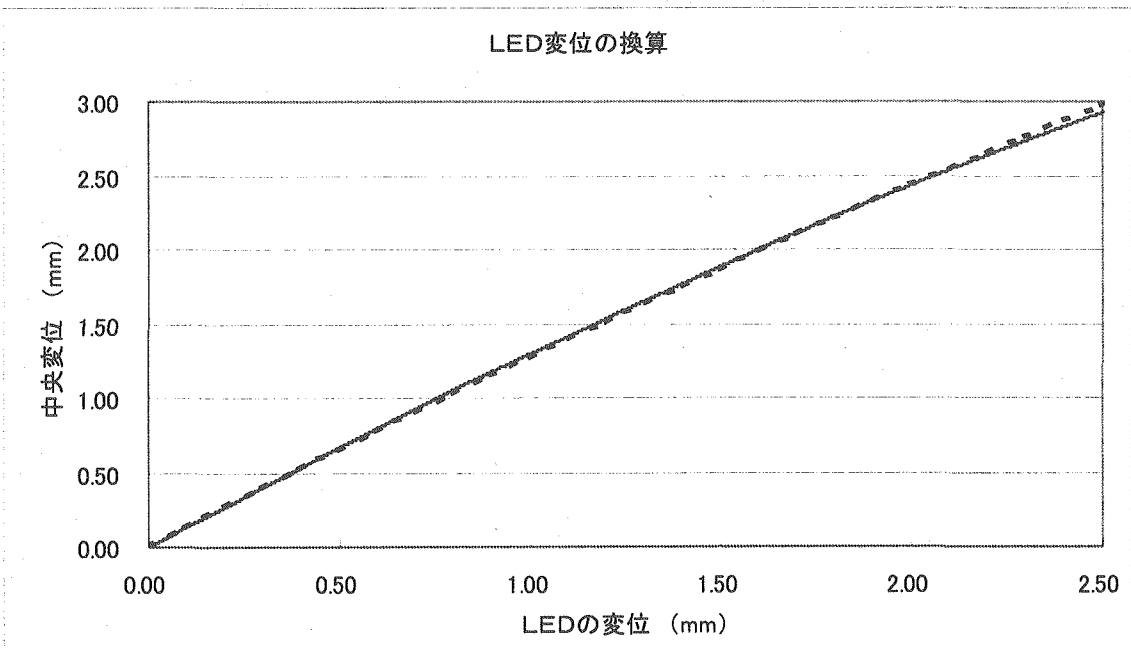

Fig. A.11 Relation between the position of the specimen measured by the LED system and the position of specimen center. The solid and dotted lines are corresponds to the measurement and calculation, respectively.

図Ａ．１２に本装置の概観写真と試験後の試験片を示す。また、図Ａ．１３には、超小型微小破壊靭性試験片であるＤＦＭＢをステージにセットした様子及びチャンバーをとして、ガラス窓の外から試験中の内部を撮影した写真を示す。

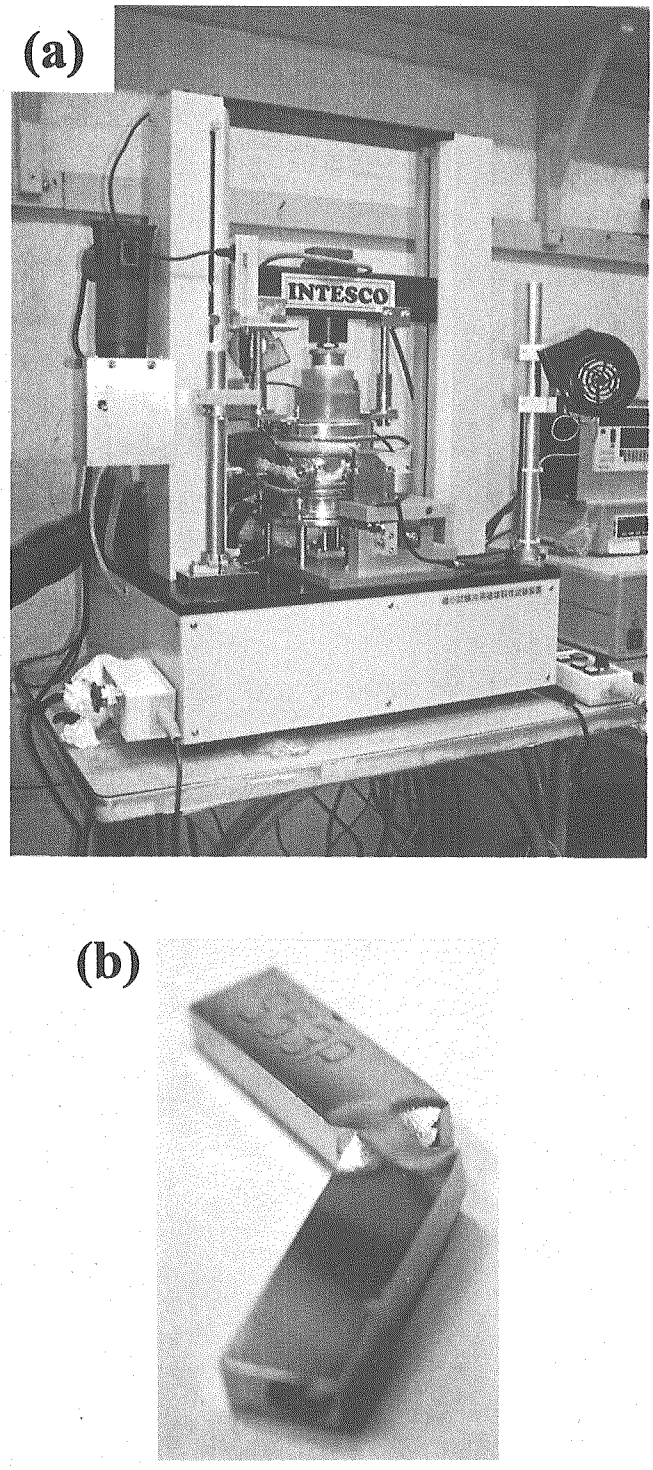

Fig. A.12　Photograph of this new machine for the fracture toughness tests of small bend type specimens. (a) appearance of new machine, (b) 1/3PCCVN specimens after the tests.

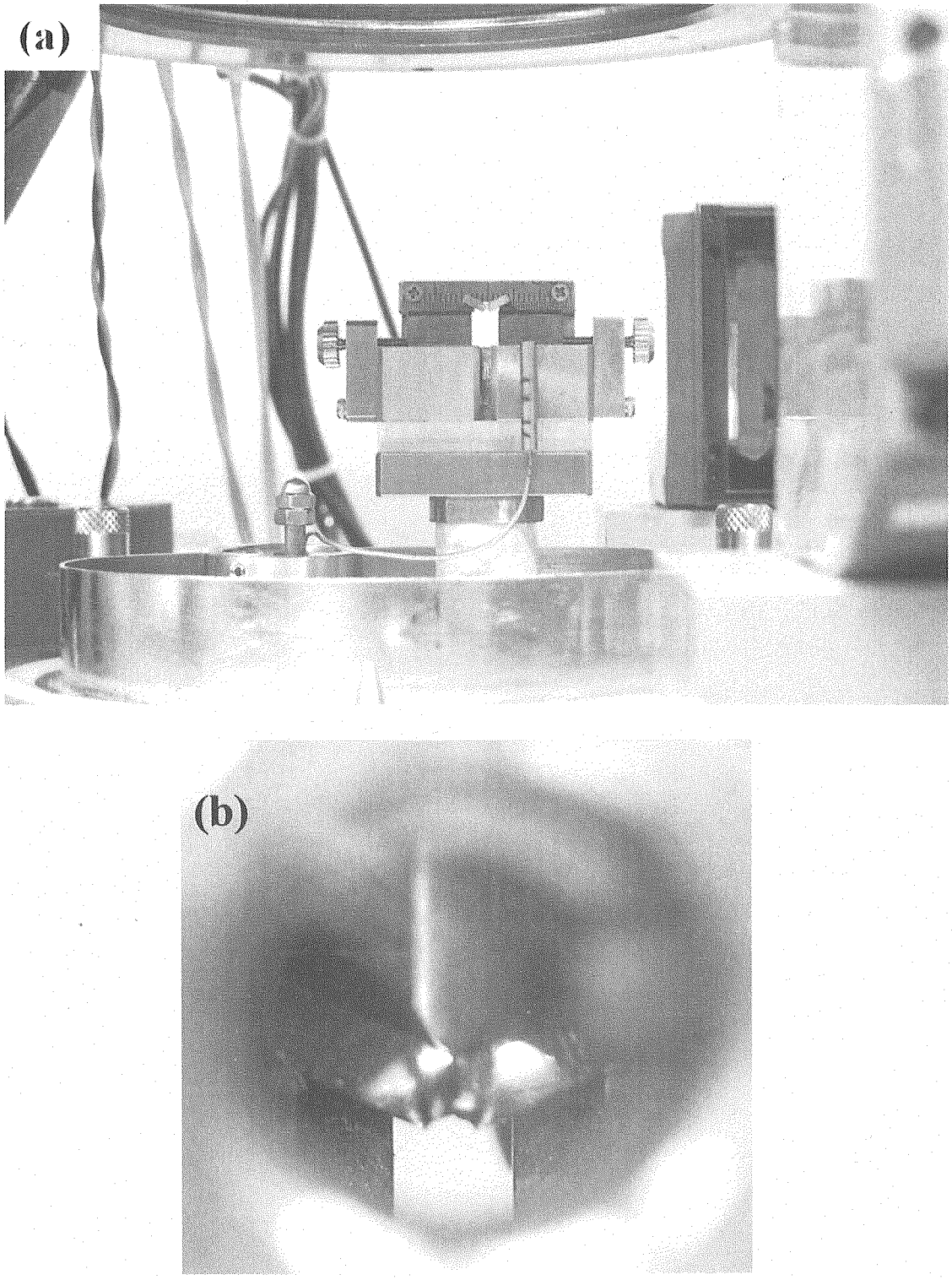

Fig. A.13 (a) Appearance of small size specimen, DFMB, on the specimen stage of the new machine after the test, (b) the DFMB specimen during the test, observed from the view window of the chamber.

A. 6　まとめ

本章では、試料の変位の測定法とその精度を検討した。
下記に、性能等を簡潔に纏め、本評価試験において得た知見等から、今後のコールド試料試験及びホット試料用試験に役立てる。

1．本装置をコールドの試験装置として用いる場合の注意点

（1）制御可能な温度は－１８０℃から３００℃であった。－１８０℃以下ではPID制御が困難であった。

（2）光学的変位測定（ＬＥＤ）を用いる場合、－１５０℃以下になると、液体窒素の噴出孔から、蒸気だけでなく、液体の塊の発生によって、試料変位測定に影響が生じた。

（3）ＬＥＤを用いる場合はガラス窓の曇り防止に留意する。槽内、及びLN_2用の配管を含んだ部分を十分に乾かす必要があった。

（4）A.５節で述べた、ＬＥＤ信号の変位量の変換に関しては、さらにいくつかのケース（サイズの異なる場合等）について調べる必要がある。

2．ホット用試験装置への反映事項

（1）　変位測定に関しては、次のことを留意する必要がある。

(a) –150℃以下での温度領域では、ＬＥＤの光学的測定はやや困難である。

(b) 光学的測定は、画像データを取り込んで解析することが望ましい。

(c) 変位の測定部は、できる限り、サンプルの近くが望ましいので、差動トランス方式を採用する。(MicroStrain 社　DVRT)

（2）装置の機構と構造

(a)液体窒素用の電磁弁は本体と分離する。(振動が伝わるのを避ける)

(b)恒温槽はロードセルの動きと独立にする。(使いやすさのため)

(c) ガラス窓曇り防止の対策　＝　ガスフロー、加温の改良。

(注：これら(1)と(2)は、ホット用試験装置の設計・製作に基本的に反映させた。)

（3）残された整備

(a)データ処理ソフトの整備が必要である。

(b)ＤＦＭＢ試験片の延性脆性遷移温度はかなり低いことから、液体窒素以下での試験も必要である。